

## Article

# Three-Dimensional Groundwater and Geochemical Reactive Transport Modeling to Assess Reclamation Techniques at the Quémont 2 Mine, Rouyn-Noranda, Canada

Mohamed Jalal El Hamidi <sup>1,2</sup>, Abdelkabar Maqsoud <sup>1,\*</sup>, Tikou Belem <sup>1</sup>  and Marie-Elise Viger <sup>3</sup>

- <sup>1</sup> Institut de Recherche en Mines et Environnement (IRME), Université du Québec en Abitibi-Témiscamingue (UQAT), Rouyn-Noranda, QC J9X 5E4, Canada; elhamidi@emi.ac.ma (M.J.E.H.); tikou.belem@uqat.ca (T.B.)
- <sup>2</sup> Laboratoire d'Analyse et de Modélisation de L'Eau et des Ressources Naturelles (LAMERN), Mohammadia School of Engineers, Mohammed V University in Rabat, Agdal 765, Morocco
- <sup>3</sup> Fonderie Horne—Glencore, Rouyn-Noranda, QC J9X 5B6, Canada; marie-elise.viger@glencore.ca
- \* Correspondence: abdelkabar.maqsoud@uqat.ca

**Abstract:** Many countries employ mining and ore processing techniques to concentrate and extract precious natural resources. However, the slow leaching of numerous dissolved elements and compounds from large quantities of waste rock and mine tailings can significantly threaten groundwater quality in the affected region. When exposed to oxygen and water, sulfide minerals in mine tailing oxidize, potentially forming acid mine drainage (AMD). Various reclamation techniques can inhibit AMD generation, including monolayer cover combined with an elevated water table (EWT), hydraulic barrier, and cover with capillary barrier effect (CCBE). Selecting the most suitable technique requires consideration of site-specific hydrogeological conditions (e.g., water table depth) and available cover materials. Numerical modeling tools such as PHT3D and MT3D can help identify optimal reclamation methods during preliminary planning stages. The 119-hectare Quémont 2 mine site near Rouyn-Noranda city will undergo reclamation following the closure of its tailings storage facilities (TSF). A three-dimensional numerical groundwater and solute-transport model were constructed and calibrated to simulate the site's hydrogeological behavior post-closure, enabling selection of the most effective AMD control technique. Subsequently, a three-dimensional multicomponent reactive transport model incorporating various cover designs was developed, with simulations considering climate change impacts. The PHT3D model code, which integrates the PHREEQC geochemical model with the MT3D three-dimensional transport simulator, was employed to evaluate cover performance on the Quémont 2 TSF. Four reclamation configurations were tested: Cell #1 (80 cm single-layer clay cover), Cell #2 (60 cm single-layer clay-sand cover), Cell #3 (60 cm single-layer clay-silt cover), and Cell #4 (120 cm multilayer clay-sand-clay sequence). Simulations were conducted under various climate change scenarios (Representative Concentration Pathways—RCPs 2.6, 4.5, and 8.5). This paper describes the numerical model, cover materials, and modeling results both with and without covers. Results indicate that Cells #1 and #4, completely reduced sulfate in groundwater, suggesting these configurations would provide the most effective reclamation solutions for the Quémont 2 mine site.



Academic Editors: Hongbiao Cui, Ru Wang, Yu Shi, Haiying Lu and Lin Chen

Received: 2 March 2025

Revised: 2 April 2025

Accepted: 10 April 2025

Published: 15 April 2025

**Citation:** El Hamidi, M.J.; Maqsoud, A.; Belem, T.; Viger, M.-E. Three-Dimensional Groundwater and Geochemical Reactive Transport Modeling to Assess Reclamation Techniques at the Quémont 2 Mine, Rouyn-Noranda, Canada. *Water* **2025**, *17*, 1191. <https://doi.org/10.3390/w17081191>

**Copyright:** © 2025 by the authors. Licensee MDPI, Basel, Switzerland. This article is an open access article distributed under the terms and conditions of the Creative Commons Attribution (CC BY) license (<https://creativecommons.org/licenses/by/4.0/>).

**Keywords:** acid mine drainage; reclamation techniques; numerical modeling; PHT3D; MT3D; PHREEQC

## 1. Introduction

The Canadian economy greatly benefits from mining mineral resources. However, mining activities produce large quantities of waste rock and mine tailings. These wastes can contain sulfide minerals such as pyrite ( $\text{FeS}_2$ ) or pyrrhotite ( $\text{Fe}_{1-x}\text{S}$ ). When exposed to oxygen and water, these minerals oxidize, generating acidity and dissolved pollutants in a process known as acid mine drainage (AMD). This oxidation reaction occurs in aqueous solution, as described by the following equation:



AMD can significantly harm the environment. In such cases, human intervention becomes necessary to limit contaminant production and prevent environmental damage to nearby ecosystems. Various management approaches and reclamation techniques are available, with selection depending on factors such as climate conditions, water budget, water table depth, and material availability [1–4].

Techniques used for mine site reclamation include an oxygen and water barrier [5]. In humid climates, typical of most Canadian regions, reducing oxygen availability by limiting oxygen diffusion is often most effective [6–8]. Water cover can be employed to reduce oxygen flux reaching reactive mine wastes (tailings or waste rocks) [9–11]. However, a key drawback of water covers is the challenge of maintaining the long-term physical stability of containment infrastructure [12,13].

The monolayer cover combined with an elevated water table (EWT) has been proposed as an alternative to water covers for tailings storage facilities (TSF) reclamation [14–24]. This method maintains high saturation levels in AMD-generating tailings by raising or maintaining the water table to keep reactive tailings highly saturated, thereby preventing oxygen diffusion [16,19,22,23,25–31].

Another approach to establishing an oxygen barrier involves covering the area with organic wastes such as wood trash, straw mulch, or other oxygen-consuming materials [32,33].

Cover with capillary barrier effects (CCBE), as described in [34–38], effectively reduce oxygen migration by using capillary barrier effects to minimize vertical water flow at interfaces. This is achieved by exploiting the contrast in hydrogeological properties (water retention curve and saturated hydraulic conductivity) between overlaid materials (fine-grained over coarse-grained). The capillary barrier effect maintains near saturation in the fine-grained material layer when it is overlaid by a coarse-grained material layer.

Hydraulic barriers represent another strategy to reduce water infiltration. Geomembranes, geosynthetic materials, and compacted clay can all create effective hydraulic barriers.

The REGENERE Chair's research program aims to identify the optimal reclamation scenario for the Quémont 2 TSF, which is expected to reach maximum capacity between 2022 and 2024 [39]. This site was selected due to its proximity to Rouyn-Noranda's urban center and Dufault Lake. Effective TSF reclamation is essential for environmental protection and requires assessment of the local hydrogeological and geochemical framework to support appropriate technique selection.

Previous studies have employed laboratory and field experiments, along with monitoring, to evaluate mine site reclamation performance. The effectiveness of selected approaches over short and long terms can be assessed using numerical simulations of water flow and reactive transport under various scenarios [16,20,22,40–42].

The Quémont 2 mine site has been extensively studied in recent years to identify its hydrogeological and hydrochemical behaviors [39,43–46]. Additionally, field and laboratory tests have evaluated different mine site reclamation approaches [47–49].

Analyzing the impact of TSF reclamation on the hydrogeological and hydrochemical behaviors of the Quémont 2 mine site is crucial. This analysis can be performed through hydrogeological and transport modeling of the site, which constitutes the goal of this paper.

## 2. Site Description

The Quémont 2 TSF, owned by Glencore Fonderie Horne, is located north of Rouyn-Noranda's urban perimeter (Abitibi-Témiscamingue, Québec) between latitudes  $48^{\circ}27' N$  and  $48^{\circ}26' N$  and longitudes  $79^{\circ}00' W$  and  $78^{\circ}97' W$  (Figure 1).

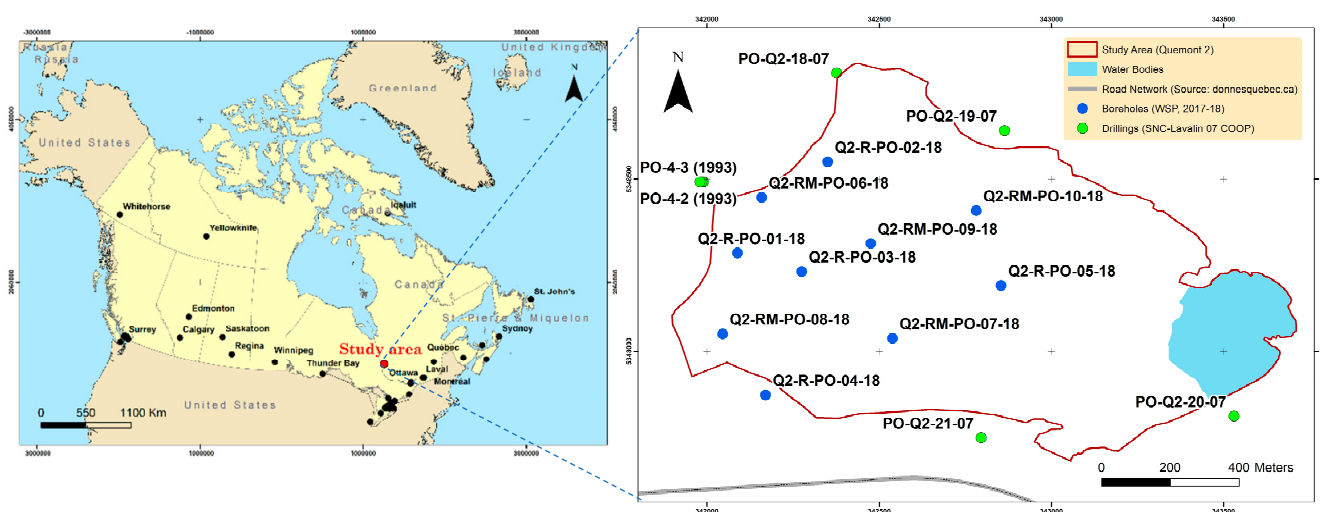


**Figure 1.** Location map of the study area.

Fonderie Horne has operated since 1927, processing copper. With over 90 years of existence, it proudly holds the title of the only copper foundry in Canada “<https://www.fonderiehorne.ca/> (accessed on 19 November 2021)”. Between 1949 and 2018, the TSF nearly reached its storage capacity, receiving more than 7.6 Million tons (Mt) of sulfide tailings, 14.2 Mt of slag, and 1.1 Mt of sludge [45].

Covering approximately 119 hectares (ha), the TSF presents unique environmental challenges due to its mine waste composition and proximity to Rouyn-Noranda's metropolitan border. This TSF borders:

- Dufault Lake, the main source of drinking water for Rouyn-Noranda;
- Osisko Lake, previously contaminated by smelting activities, mine tailings storage, and municipal wastewater.

The regional hydrogeological context of the Quémont 2 site is defined by a bedrock that is generally exposed or covered by unconsolidated glacio-lacustrine deposits.

The Quémont 2 TSF has been used successively for sulfide tailings deposition and the co-deposition of sludge and slag. These co-deposited materials consist of fresh slag generated from copper flotation at the Horne smelter concentrator and lime treatment from the weak-acid treatment unit [44]. These materials can potentially generate contaminated water, posing a risk to the health and safety of Rouyn-Noranda's population and affecting the surrounding environmental quality.

## 3. Methodology

This paper first provides an overview of the Quémont 2 site, then introduces the hydrogeological database and numerical model used to characterize and simulate the hydrogeological and hydrochemical behaviors of the Quémont 2 TSF.

### 3.1. Data Collection and Field Measurements

**Data Acquisition:** The most expensive step in establishing the database is data collection. This process involves gathering various subsurface and water resources data from the study area and incorporating them into the hydrogeological database. The data were collected from Glencore Fonderie Horne databases and several online sources, including Government of Quebec websites (e.g., “diffusion.mern.gouv.qc.ca, donnesquebec.ca, SIGÉOM” accessed on 19 November 2021). Input alphanumeric data, digitization of maps, profiles, and cross-sections, as well as spatial entities, were processed, followed by integration of attributes and descriptive semantic data into the hydrogeological database.

To determine precise properties of various subsurface units within the TSF, cross-sections, drilling, and survey data provided by [46] were utilized. Twelve drill holes with depths ranging from 4 to 16 m were examined across the TSF. Additionally, high-precision topographic data from the Glencore database, provided in AutoCAD format (.DWG), determined the TSF altitude.

A geophysical study conducted near the old TSF in 2021 by [44] employed two main techniques: Ground-Penetrating Radar (GPR) and Electrical Resistivity Tomography (ERT). GPR was deployed in Common Mid-Point mode to determine the propagation speed of Electromagnetic Waves (EMW) within the tailings. This approach enabled the estimation of surface water content by leveraging the established relationship between EMW propagation speed, dielectric constant, and water content. The results demonstrated the effectiveness of GPR in assessing surface moisture content and identifying physical discontinuities, particularly within the dams surrounding the tailings. ERT mapped the subsurface and estimated physical and hydraulic properties of the mine tailings. Through Archie’s Law application, a cross-sectional map of porosity distribution was developed. Furthermore, by combining resistivity data with the Kozeny–Carman equation, a hydraulic conductivity highlighted a strong spatial heterogeneity of these properties.

The variables of interest in this study include reservoir geometry (topography as Digital Elevation Model (DEM), bottom, aquifer thickness, hydrogeological units), hydrogeology, hydro-climatology, and groundwater quality parameters such as pH and water temperature ( $T^{\circ}$ ). These variables were obtained from multiple data sources and relevant reports (Tables 1 and 2) and were used for conceptual model preparation.

To ensure accurate integration and representation of spatial data in the GIS, all collected geolocation data originally defined using the WGS84 coordinate system were converted to the Canadian NAD 1983—MTM 10 projection using ArcGIS software (Version 10).

**Field measurements:** In November 2021, additional investigations were conducted as part of this study to measure hydraulic head, temperature, and water electrical conductivity (Research Institute on Mines and the Environment (IRME) laboratory, Rouyn Noranda, QC, Canada). In 2018, Solinst Levelogger Edge probes were installed in wells Q2-RMPO-09-18, Q2-R-PO-03-18, Q2-RM-PO-06-18, and Q2-R-PO-01-18 for hydraulic heads monitoring [44]. Data were collected between 5 November 2020, and 3 June 2022, at hourly intervals. Additionally, a Barologger installed at well Q2-R-PO-03-18 monitored atmospheric pressure, enabling correction of piezometric levels obtained with the Levelogger probes.

**Table 1.** Data products of geology/reservoir are used for the preparation of the conceptual model.

Data	Data Types	Conceptual Model	Sources	Values or Year of Data Production	
Geology/ Reservoir	Subsurface: sludge and slag, tailings, glacio-lacustrine deposits, and the rock	■ 4 Layers, phreatic and semi-captive layers	■ [39]	■ 2018	
		■ No flow on the north	■ [39]	■ $Q = 0 \text{ m}^3/\text{day}$ (2018)	
		■ No flow on the south	■ [39]	■ $Q = 0 \text{ m}^3/\text{day}$ (2018)	
		■ Newman conditions on the southeast (Outflow)	■ Calculated in 2022	■ $Q = 216 \text{ m}^3/\text{day}$ (2020)	
		■ Newman conditions on the east limit (Outflow)	■ Calculated in 2022	■ $Q = 0.855 \text{ m}^3/\text{day}$ (2020)	
		■ Dirichlet condition: Constant-head on the west (Catch Basin)	■ [44]	■ $H = 323.5 \text{ m}$ (2020)	
		■ $Z(x,y)$ Ground/ocean	■ Glencore, Fonderie Horne database		
		■ Topographic maps (AutoCAD Format).			
		Boundary conditions	■ Contour line and point	■ [50]	■ 2022
			■ DEM (1/20,000)	■ [50]	
	■ ESRI Map		■ ArcGIS Software		
	■ $U1(x,y)$ top of the mine tailing: 9 boreholes.		■ [39]	■ 2018, 2017 ■ Values per point (x, y, levels)	
	■ $U2(x,y)$ top of the glacio-lacustrine deposits, mainly clays: 9 boreholes.	■ [39,51,52]	■ 2018, 2007, and 1993 ■ Values per point (x, y, levels)		
	■ $U3(x,y)$ top of the fractured rock: 10 boreholes.	■ [39,52]	■ 2018, 2017, 2007 ■ Values per point (x, y, levels)		
■ $B(x,y)$ top of the bedrock: 10 boreholes reach the bottom.	■ [39,52]	■ 2018, 2017, 2007 ■ Values per point (x, y, levels)			

Humidity cell tests were conducted to evaluate the hydrochemical behavior of the sulfide tailings, as well as sludge and slag materials, at the Research Institute on Mines and the Environment (IRME) laboratory in Rouyn-Noranda, QC, Canada. Geochemical parameters were analyzed at the SGS (Société Générale de Surveillance) laboratory using ICP-AES and ICP-MS to assess the metal leaching potential of elements such as As, Cu, Fe, Pb, and Zn.

Graphical representations were generated using Microsoft Excel (Version 2019). Groundwater flow simulations and geochemical modeling were carried out using MODFLOW 2000, PhT3D, and MT3D, implemented through the Visual MODFLOW interface (Version 2014).

**Table 2.** Data products of hydrogeology, hydro-climatology, and groundwater quality used for the preparation of the conceptual model.

Data	Data Types	Conceptual Model	Sources	Values or Year of Data Production
Hydrogeology	Hydrodynamic parameters	<ul style="list-style-type: none"> <li>Permeability, K (m/s): 10 pumping tests</li> </ul>	<ul style="list-style-type: none"> <li>[39]</li> </ul>	<ul style="list-style-type: none"> <li>2018</li> </ul>
	Piezometry and depth	<ul style="list-style-type: none"> <li>Four wells: water Depth (m).</li> <li>Four wells: piezometric level (m).</li> </ul>	<ul style="list-style-type: none"> <li>Collected data</li> </ul>	<ul style="list-style-type: none"> <li>From 2020 to 2022</li> </ul>
Hydro-Climatology	Precipitation and Temperature	<ul style="list-style-type: none"> <li>Rouyn station completed by surrounding stations</li> </ul>	<ul style="list-style-type: none"> <li>[53]</li> </ul>	<ul style="list-style-type: none"> <li>From 2020 to 2022</li> </ul>
	Projected precipitation and temperature	<ul style="list-style-type: none"> <li>Location: Latitude: 48,27° N, Longitude: 78.99° W</li> </ul>	<ul style="list-style-type: none"> <li>[54]</li> </ul>	<ul style="list-style-type: none"> <li>From 2020 to 2100</li> </ul>
	AMD, Catch basin	<ul style="list-style-type: none"> <li>Drain</li> </ul>	<ul style="list-style-type: none"> <li>[39]</li> </ul>	<ul style="list-style-type: none"> <li>2018</li> </ul>
Groundwater Quality	Physical and chemical parameters	<ul style="list-style-type: none"> <li>Geochemical results of groundwater in µg/L from 10 wells</li> </ul>	<ul style="list-style-type: none"> <li>[45]</li> </ul>	<ul style="list-style-type: none"> <li>2019, 2020</li> </ul>
		<ul style="list-style-type: none"> <li>Groundwater quality analysis in µg/L from 10 wells</li> </ul>	<ul style="list-style-type: none"> <li>[39]</li> </ul>	<ul style="list-style-type: none"> <li>2018</li> </ul>

### 3.2. Climate Data

Climate data were obtained from the Rouyn meteorological station [53]. In 2020, the average annual precipitation was 882.8 mm, while the average minimum and maximum monthly temperatures were  $-17^{\circ}\text{C}$  (in February) and  $26^{\circ}\text{C}$  (in July), respectively. The region's climate is characterized by cold winters and warm summers.

This assessment incorporates a combination of regional climate modeling projections data generated by the Government of Canada [54] and a local observational dataset for precipitation (P) and temperature (T) specific to the study area. The analysis involved extracting a time series of P and T variables from 2006 to 2100. MATLAB software (Version R 2024b) was employed to process and extract time data from NetCDF (Network Common Data Form: "[www.unidata.ucar.edu/software/netcdf](http://www.unidata.ucar.edu/software/netcdf)" (accessed on 1 January 2022)) files (.nc). Data extraction was conducted for a specified latitude and longitude coordinates, covering the entire timeframe from 2006 to 2100.

Time series plots based on the climatic data, which summarize the most up-to-date knowledge on the study area's climatology, are presented in Figure 2a,b. These figures illustrate the predicted evolution of P and T for the coupled model intercomparison project 5 (CMIP5) climate model, considering multiple scenarios used to study the future impact of climate change (CC). The scenarios include the Representative Concentration Pathways (RCPs) 2.6, 4.5, and 8.5, which have been analyzed and edited for this study.

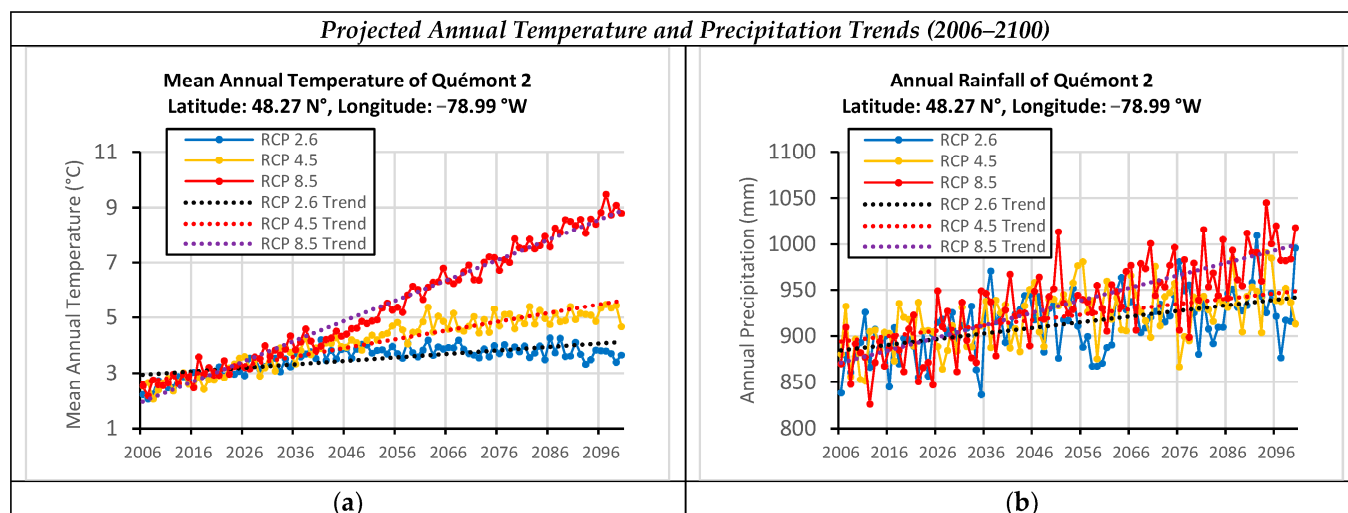


**Figure 2.** Temperatures (a) and precipitations (b) over time (2006–2100) in the study area for RCP 2.6, RCP 4.5, and RCP 8.5.

For all three scenarios, these graphs clearly show an upward trend in both temperatures and precipitation, indicating increases in these variables over time.

### 3.3. Hydrogeological Database

A geodatabase was created using data collected from various organizations and studies, providing detailed information on surface water and groundwater resources, including geology, piezometry, geometry, and quality. This database generates decision-support thematic maps and diagrams. The resulting thematic layers were organized to meet the needs of managers and decision-makers, covering the study area's location, administration, hydrology, climatology, hydrogeology, and aquifer geometry. This organization facilitates easy consultation, customization, and replication of information across different water resources management applications. Additionally, the conceptual model of the study area has been integrated into this database.

### 3.4. Hydrogeological Setting

At the Quémont 2 TSF, four piezometers were equipped with data loggers to continuously monitor groundwater levels from 5 November 2020 to 3 June 2022.

The hydrostratigraphic units presented in this section were established using borehole logs from previous studies [51,52,55] and survey campaign conducted in 2017 and 2018 [39]. A total of seventeen boreholes, with depths ranging from 4 m to 41 m, were utilized across the Quémont 2 TSF.

A three-dimensional (3D) model was developed based on available data concerning the non-reactive sludge and slag material, Quémont 2 tailings, and underlying structural units (rock and glacio-lacustrine deposits) (Figure 3). The Quémont 2 TSF is primarily characterized by four hydrogeological units, extending from the bottom to the surface.

#### 3.4.1. Unit 1 (Rock)

The rock unit at the Quémont 2 site is relatively homogeneous. Based on observations made during drilling, the bedrock beneath the TSF consists of basalt and andesite, exhibiting varying degrees of alteration.

The till unit has not been considered in this research, as it lies outside the study area.

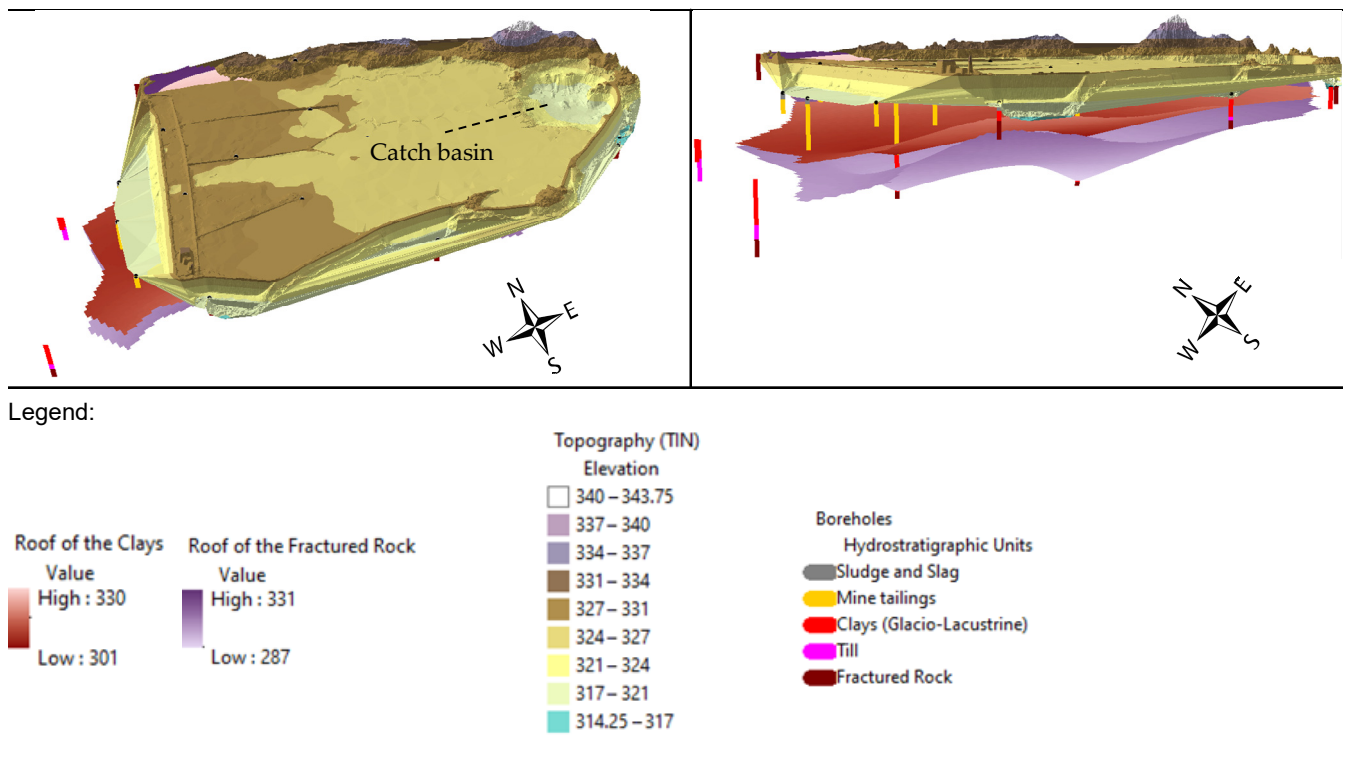


**Figure 3.** Three-dimensional (3D) model configuration of the Quémont 2 TSF.

#### 3.4.2. Unit 2 (Glacio-Lacustrine Deposits)

The glacio-lacustrine deposits unit consists of clayey silt and clay layers. Due to limitations in the available data for Quémont 2, it is not possible to distinctly differentiate between a clay unit and an overlying clayey silt unit. Therefore, for modeling simplicity, these two units have been grouped. The clay deposits are characterized by rhythmites of clay and silt, with a thickness ranging from 0 m to 15 m. The thickness of the clay deposit units is shown on Figure 3, between the garnet and purple raster layer.

#### 3.4.3. Unit 3 (Mine Tailings)

Unit 3 consists of mine tailings accumulated at the Quémont 2 site, primarily composed of silty materials with low compactness. The thickness of the tailings is shown in Figure 3, between the garnet layer and the DEM raster layer. Based on drilling data, the mine tailings thickness ranges from 0 m to 25 m, with the greatest thickness observed in the center of the TSF. This unit is present throughout the entire TSF, except in the northern part.

#### 3.4.4. Unit 4 (Sludge and Slag)

Mine tailings (unit 3) are covered by a mixture of sludge and slag materials. According to [56], sludge has a much finer grain size compared to slag and is generally less dense. The average thickness of this mixed unit is approximately 1.6 m, which was determined by calculating the difference between the DEM and the mine tailing unit.

### 3.5. Hydrodynamic Parameters

The hydraulic conductivity values obtained through the interpretation of the slug-test method [57] range from  $3.34 \times 10^{-7}$  m/s to  $3.81 \times 10^{-6}$  m/s in the mine tailings unit, with a geometric mean value of  $1.4 \times 10^{-6}$  m/s (Table 3).

**Table 3.** Hydraulic conductivity throughout the Quémont 2 TSF.

Unit	Borehole	Hydraulic Conductivity (m/s)		
		Test 1	Test 2	Geometric Mean
Unit 1 (Rock)	01–18	$9.97 \times 10^{-7}$	$7.36 \times 10^{-7}$	$6.6 \times 10^{-7}$
	02–18	$2.17 \times 10^{-7}$	$1.26 \times 10^{-7}$	
	03–18	$4.42 \times 10^{-6}$	n/d	
	04–18	$3.41 \times 10^{-7}$	$3.25 \times 10^{-7}$	
	05–18	$1.5 \times 10^{-6}$	$1.54 \times 10^{-6}$	
Unit 4 (Mine Tailings)	06–18	$3.5 \times 10^{-6}$	$3.81 \times 10^{-6}$	$1.4 \times 10^{-6}$
	07–18	$1.2 \times 10^{-6}$	$1.16 \times 10^{-6}$	
	08–18	$2.7 \times 10^{-6}$	$3.32 \times 10^{-6}$	
	09–18	$3.55 \times 10^{-7}$	$3.34 \times 10^{-7}$	
	10–18	$9.11 \times 10^{-7}$	$1.12 \times 10^{-6}$	

In the rock unit, hydraulic conductivity varies between  $1.26 \times 10^{-7}$  m/s and  $4.42 \times 10^{-6}$  m/s, depending on the degree of rock fracturing, with a geometric mean value of  $6.6 \times 10^{-7}$  m/s for the rock mass as a whole. We acknowledge that the density and distribution of fractures significantly influence hydraulic conductivity values in fractured rock units. In our study, we considered the degree of fracturing as a critical factor when estimating hydraulic conductivity. However, we did not directly measure the fracture density.

We also recognize that slug tests in fractured rock can be misleading if the tested volume is not representative of the overall rock mass. To address this, we conducted multiple slug tests across different locations to obtain an average hydraulic conductivity value.

In addition, pumping tests from previous studies [57–59], as reported in the WSP report [39], provided permeability values for the clay unit. A typical value of around  $10^{-9}$  m/s is generally considered representative for the glacio-lacustrine deposits unit.

### 3.6. Kinetic Test Method

Humidity cell tests performed by [43] were used to evaluate the geochemistry of the Quémont 2 tailing storage facility, specifically to accelerate sulfide mineral oxidation and acid generation. The test procedure involved weekly wetting and drying cycles, with 1 L of deionized water being flushed over 1 kg of the studied material. At the end of each humidity cell test cycle, the water flush was analyzed for various geochemical parameters to assess oxidation rates, alkalinity generation, and the potential for metal leaching (As, Cu, Fe, Pb, and Zn).

These tests were conducted over 16 cycles (105 days) on material from both the sludge/slag and the mine tailing. The results showed that the sludge/slag exhibited generally lower pH values (ranging from 6.2 to 7.0) compared to the mine tailings (ranging from 7.0 to 8.3) over the 105-day period. The electrical conductivity of water from the mine tailings ranged between 944  $\mu\text{s}/\text{cm}$  and 3750  $\mu\text{s}/\text{cm}$ , consistently higher than that from the sludge/slug, except during the final leaching phase.

The sludge/slag produced higher Zn and Cu concentrations compared to the mine tailings. Specifically, the Zn concentration reached up to 0.13 mg/L in the mine tailings and up to 2.25 mg/L in the sludge/slug. For Cu, concentrations were up to 0.03 mg/L in the mine tailings and up to 4.34 mg/L in sludge/slug. However, after 42 days, the Zn concentration in the mine tailings became acceptable ( $<1$  mg/L), in accordance with Directive 019 requirements [60], established by the Ministry of the Environment of Quebec, Canada. These regulations ensure that mining activities adhere to strict environmental protection measures to minimize the impact of tailings and wastewater on the environment.

A significant difference in sulfur (S) concentrations was observed between the sludge/slag and the mine tailings, with values ranging from 12 mg/L to 1018 mg/L.

Iron (Fe) concentrations in both the sludge/slag and mine tailings remained very low, either close to or below the detection limit of 0.007 mg/L throughout the tests.

### 3.7. Model Construction and Boundary Conditions

The conceptual model was developed based on the hydrogeological database and field data, while the mathematical model was constructed to simulate transient groundwater flow for the Quémont 2 TSF from 2020 to 2100 (Figure 4). The conceptual model and model discretization were developed using Visual MODFLOW software (Version 2014). In the plan view, the simulation domain was discretized into a grid consisting of 22,800 grid cells, with a layout formed by 190 columns and 120 rows of 10 m × 10 m cells, aligned along the north–south (NS) and west–east (WE) directions (Figure 5a). Vertically, the model grid incorporates four layers of varying thicknesses, corresponding to the Quémont 2 TSF hydrostratigraphic units described earlier (Figures 3 and 5b).

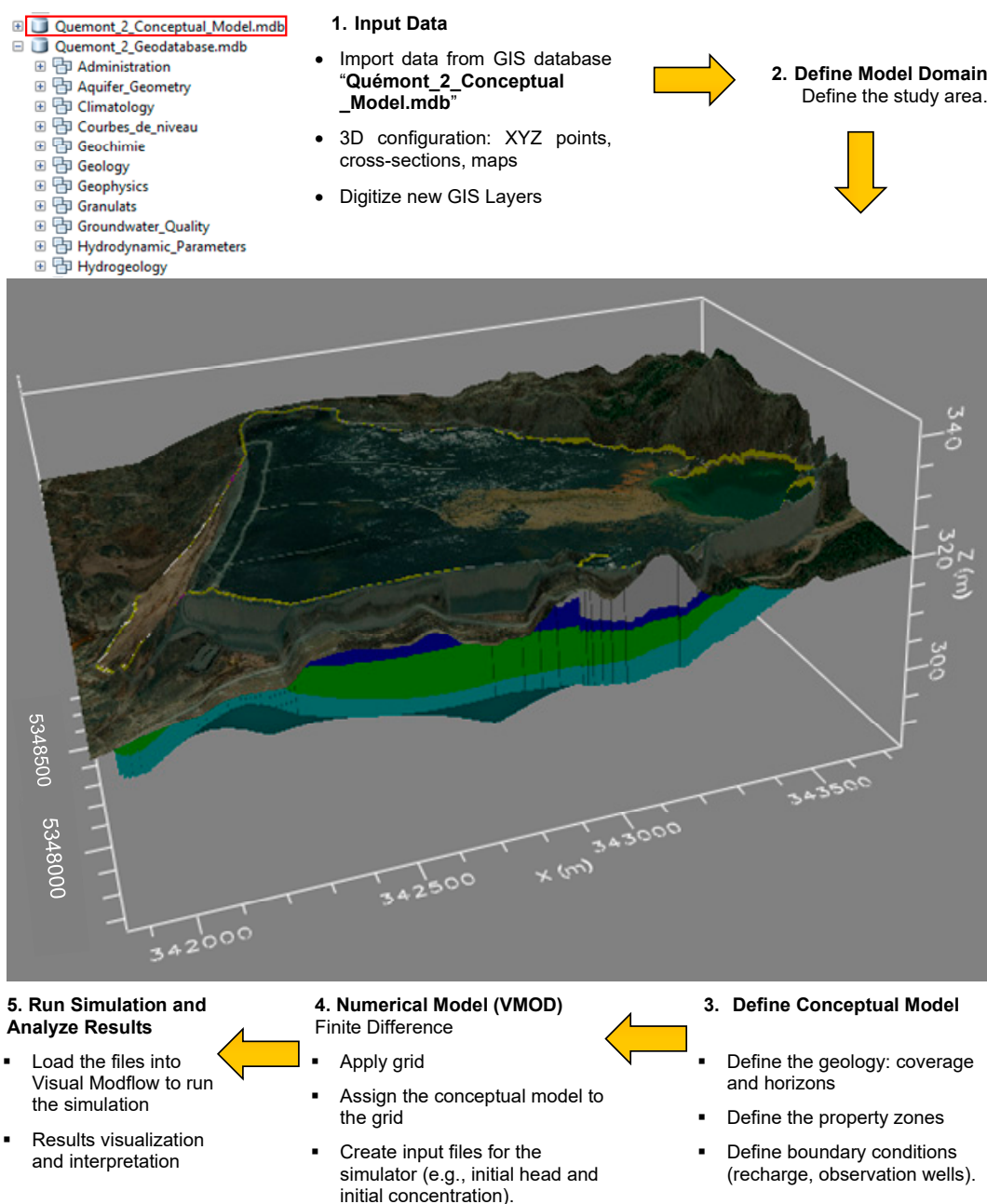
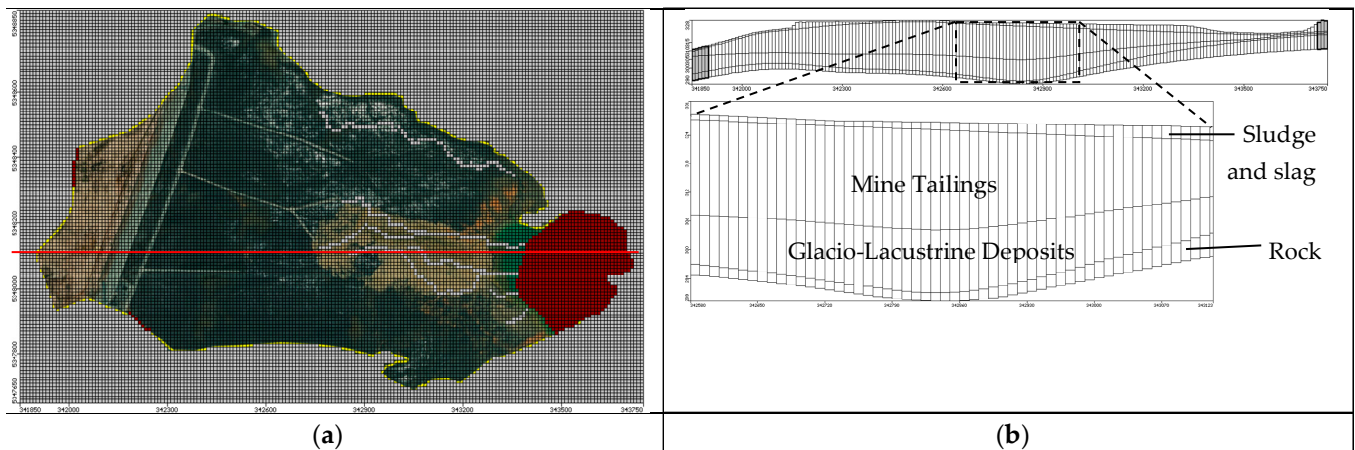


Figure 4. Numerical and conceptual model workflow using Visual MODFLOW software, Quémont 2.



**Figure 5.** The model discretization of Quémont 2 TSF, showing inactive zone (gray) and active zone. (a) Plan view of the spatial discretization for the numerical model and location of the cross-section profile (b) A cross-section of the research area from west to east, displaying the hydrogeologic units and a vertical spatial discretization of the study area.

The modeled area spans a total of 119 ha, with the base elevation of the model set at 285 m above sea level and a maximum elevation of 332 m at the surface. The model grid includes a mesh of 11,953 active cells, capturing the subsurface structure in detail. The domain encompasses layers representing rock, glacio-lacustrine deposits, Quémont 2 tailings, and sludge/slag tailings cover layers, as illustrated in Figure 5b, which provides a cross-section of the model domain and the thicknesses of its various layers.

### 3.8. Groundwater Flows and Contaminant Transport Modeling

Visual MODFLOW software [61], a fully integrated 3D finite-difference subsurface flow model based on the diffusivity equation, was used to simulate groundwater flow and contaminant transport over time.

The USGS (United States Geological Survey) groundwater flow model MODFLOW and the MT3D contaminant transport model, along with add-on packages (e.g., PHT3D, MODPATH, ZONE BUDGET, and FMBUDGET), are integrated into the widely used Visual MODFLOW software to simulate a complex three-dimensional groundwater flow at the study site.

For this study, MODFLOW 2000 [62] was chosen to assess three-dimensional groundwater flow in a porous medium (Figure 6). The groundwater flow partial differential equations were solved using the Bi-Conjugate Gradient Stabilized (Bi-CGSTAB) acceleration technique in Visual MODFLOW. The convergence of the calibrated model's matrix solver was assessed using head changes of 0.01 m and residual criteria of 0.001 m.

A three-dimensional numerical groundwater flow model was calibrated under steady-state and transient groundwater flow conditions, solving Equation (2) [63] for a 576-day period, from 5 November 2020 to 3 June 2022. The model also predicts hydraulic head and contaminant concentration in the Quémont 2 TSF from 2021 to 2100 under three different CC scenarios (RCPs 2.6, 4.5, and 8.5), as well as the water balance over time.

$$\frac{\partial}{\partial x} \left( K_{xx} \frac{\partial h}{\partial x} \right) + \frac{\partial}{\partial y} \left( K_{yy} \frac{\partial h}{\partial y} \right) + \frac{\partial}{\partial z} \left( K_{zz} \frac{\partial h}{\partial z} \right) \pm W = S_s * \frac{\partial h}{\partial t} \quad (2)$$

The parameter  $K_{xx}$ ,  $K_{yy}$ , and  $K_{zz}$  represent hydraulic conductivity values along the  $x$ ,  $y$ , and  $z$ -axis directions ( $L/T$ );  $h$  denotes the potentiometric head ( $L$ );  $W$  is the volumetric flux per unit volume representing sources and/or sinks ( $T^{-1}$ );  $S_s$  is the specific storage of the porous material ( $L^{-1}$ ); and  $t$  represents time ( $T$ ).

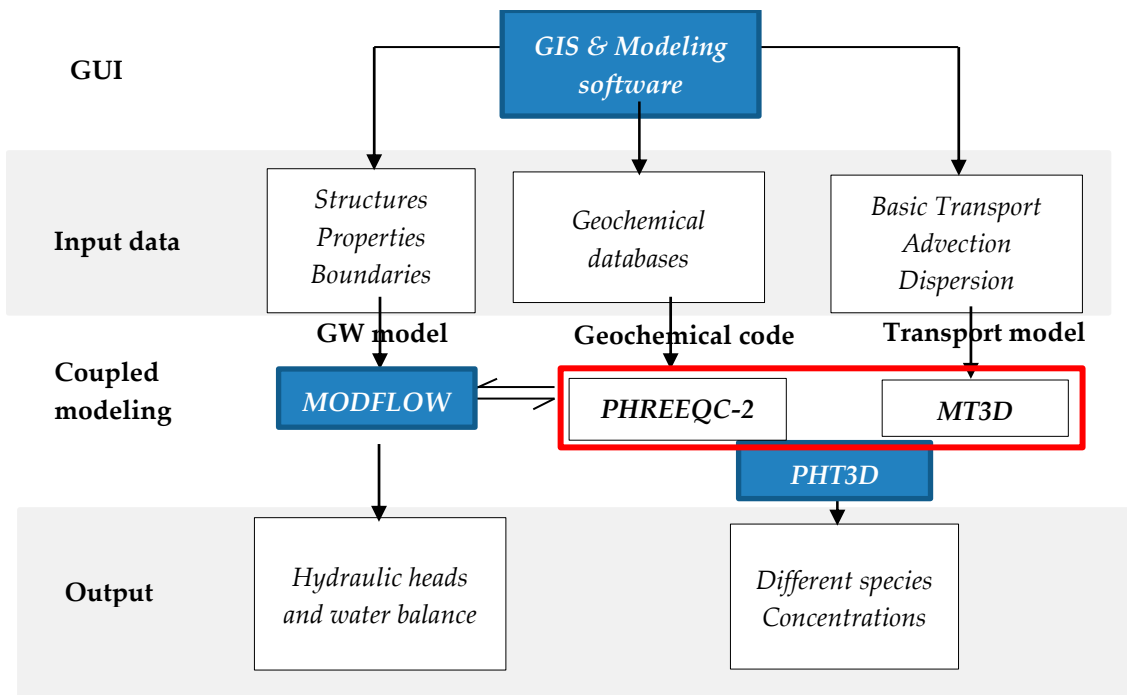


**Figure 6.** Architecture of the coupled MODFLOW/PHT3D model. The red box highlights the geochemical code (PHREEQC-2) and the transport model (MT3D), which work together to simulate reactive transport processes within the PHT3D framework.

The coupled flow and transport code (MT3D), which solves Equation (3) [64], was applied to both qualitatively and quantitatively study contaminant transport in the Quémont 2 TSF.

$$\frac{\partial C}{\partial t} = \frac{\partial}{\partial x_i} \left( D_{ij} \frac{\partial C}{\partial x_j} \right) - \frac{\partial}{\partial x_i} (V_i C) - \frac{q_s C_s}{\theta} + \sum_{k=1}^N R_k \quad (3)$$

Here,  $C$  represents the contaminant concentration in groundwater ( $ML^{-3}$ );  $T$  represents time ( $T$ );  $x_{i,j}$  denotes the position along the Cartesian coordinate axes ( $L$ );  $D_{ij}$  is the hydrodynamic dispersion coefficient tensor ( $L^2T^{-1}$ );  $V_i$  is the fluid velocity ( $LT^{-1}$ );  $q_s$  volumetric flow rate per unit volume of aquifer representing fluid sources (positive) and sinks (negative) ( $T^{-1}$ );  $C_s$  is the concentration of the source or sink flux ( $ML^{-3}$ );  $\theta$  is the porosity of the subsurface medium (*dimensionless*), and  $R_k$  ( $k = 1, \dots, N$ ) represents the rate of solute production or decay in reaction  $k$  of  $N$  different reactions ( $ML^{-3}T^{-1}$ ).

To reliably predict contaminant transport at the site, an accurate groundwater flow model must first be developed, calibrated, and validated to adequately represent site conditions.

A reactive multicomponent transport model based on MODFLOW/MT3D was recently developed by [65]. This model solves various mixed equilibrium and kinetic reactive transport problems by sequentially coupling the geochemical model PHREEQC-2 [66] with the three-dimensional transport simulator MT3D [64] (Figure 6). The model can solve both equilibrium and kinetically controlled reactions, with total aqueous component concentration serving as the main dependent variable [67,68].

The PHT3D model was selected because it allows for the addition of new reactions to those already in the database, with levels that can be established by other species. Visual MODFLOW facilitates easy formatting of Input data for both the PHT3D model (advection, dispersion, and concentration) and the MODFLOW model (geometry and permeability), and provides visualization of the model's outputs (head changes and concentrations).

Iron and sulfur were defined as the principal contaminating species for this simulation, due to their significance in AMD production. In the bedrock unit, high concentrations of iron and sulfate in the presence of oxygen and water can contribute to acidity and AMD production. According to data from wells PO-Q2-19-07, PO-Q2-22-07, Q2-R-PO-02-18, and Q2-R-PO-04-18, from summer 2020 monitoring [45], the iron concentration in the bedrock unit averages 42.5 mg/L, the sulfate concentration averages 1913.8 mg/L, and the pH averages 6.1 (Table 3).

The movement of pollutants through porous media is governed by complex mechanisms. These processes are formally described in the model, with differential equations applied using the field data provided in Table 4. The concentrations of iron, sulfur, and other components were assessed based on groundwater quality measurements, supplemented by kinetics tests conducted by [43] on Quémont 2 materials.

**Table 4.** Geochemical parameters of groundwater in 2020 [45].

N°	W19-07	W22-07	W02-18	W04-18
Fe (µg/L)	1300	42,000	17,000	11,0000
SO <sub>4</sub> (µg/L)	15,500	2,170,000	2,750,000	2,720,000
pH	5.54	6.68	6.67	5.51

For simplicity, a two-dimensional reactive transport model was established for the tailings and sludge/slugs. This study used the “wateq4f.dat” PHREEQC-2 database. Reactive transport was modeled for eight components—calcium (Ca), Arsenic (As), Cadmium (Cd), Cobalt (Co), copper (Cu), iron (Fe), lead (Pb), sulfur (S), and zinc (Zn)—in equilibrium phases, within the context of the local hydrogeologic conditions of the Quémont 2 site (Table 5). As required by PHT3D, the concentrations of these components were converted to mol/L. A constant head boundary was used for point source concentrations in this simulation. A key focus of this study was assessing the impact of varying concentrations on groundwater quality in and around the central Quémont 2 area.

**Table 5.** Transport model parameters and initial concentration (mmol/L) of aqueous components.

Parameters Unit	Values	
Effective porosity	0.3	
Longitudinal dispersivity ( $\alpha_L$ )	9	
Transverse dispersivity ( $\alpha_T$ )	3	
TRPT ratio m	0.333	
TRVT ratio m	0.0333	
Components and Concentration	Tailings	Sludge and slag
As	0.000034703	0.00004138
Cd	0.000007704	0.00043412
Co	0.000184955	0.00007432
Cu	0.000140056	0.04547887
Fe	0.001092309	0.00039395
Pb	0.000000820	0.05791506
S	31.37866500	0.37429819
Zn	0.000565922	0.02493117
pH	7.51	6.85
pe	413	598
Sulfur	0.0313 mol/L	-

## 4. Modeling Results

### 4.1. Steady-State Calibration

The calibration of the groundwater flow model involved adjusting parameters to ensure simulated results closely matched observed conditions, while maintaining parameter values within appropriate ranges. The steady-state, three-dimensional finite-difference flow model of Quémont 2 was calibrated and validated using statistical metrics including Root Mean Squared Error (RMSE), Mean Absolute Error (MAE), normalized RMSE, and percent mass balance discrepancy.

Steady-state calibration was performed by comparing simulated and measured hydraulic heads at each monitoring station (Figure 7c). The calibration results demonstrated an average correlation coefficient of 1.0, a MAE of 0.046 m, and an RMSE of 0.052 m.

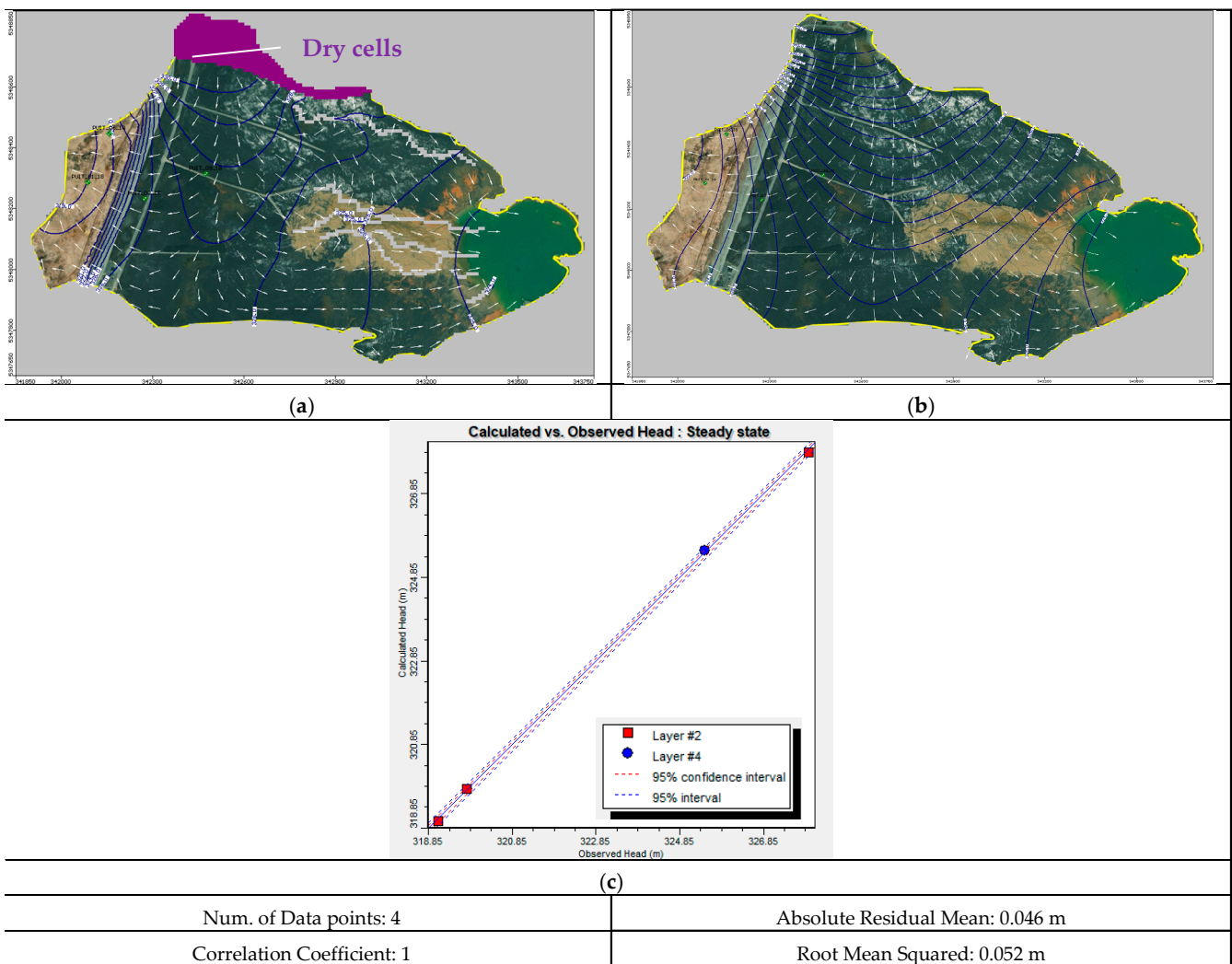


**Figure 7.** Simulated hydraulic head (m) of: (a) mine tailing, (b) rock, and (c) correlation between simulated and measured hydraulic heads for 5 November 2020. The arrows represent flow direction or vector velocities. The blue lines represent equipotential lines or hydraulic head contours.

Groundwater primarily flows from north to east, with a secondary flow component toward the west. Flow directions are illustrated by vector velocities in Figure 7. Figure 7a depicts the simulated flow patterns within the mine tailing unit, with dry cells in the northern portion of the model resulting from the absence of mine tailings in that area. Figure 7b illustrates the simulated flow within the rock unit.

#### 4.2. Transient State Calibration

The model was calibrated in the transient state using average hydraulic head measurements from 5 November 2020 to 3 June 2022. In Figure 8a, the line represents the correlation between modeled and observed results after 80 days. Piezometer probes from wells 1, 6, and 9 are located in the mine tailings (Layer 2: red points), while the probe from well 3 is located in the rock unit (Layer 4: blue points). It should be noted that the lower hydraulic head values in Figure 8a correspond to the lower hydraulic head shown in Figure 8b in the transient state, while the higher values in Figure 8a correspond to the higher hydraulic heads shown in Figure 8b.

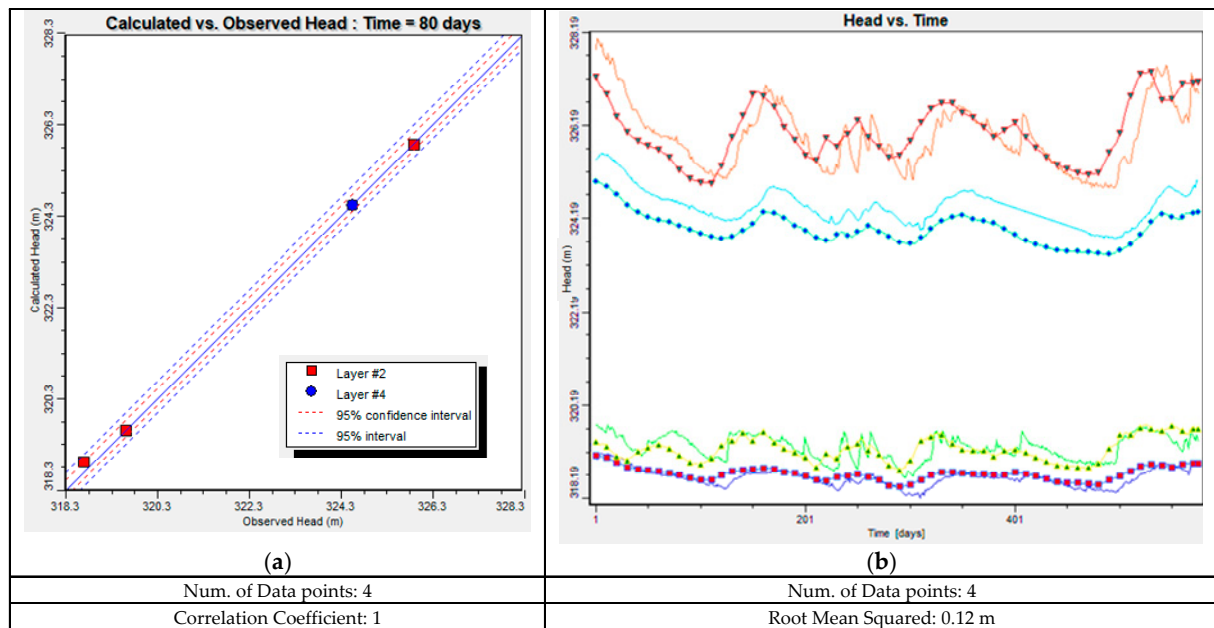


**Figure 8.** (a) Calibrated hydraulic heads comparing estimated and observed transient state in a scatter diagram (Time = 80 days), (b) simulated (line and points) and observed (line) daily hydraulic heads at observation wells 1, 3, 6, and 9 from 5 November 2020, to 3 June 2022. The orange/red line represents monitoring well 9, light blue line shows monitoring well 3, green line represents monitoring well 6, and purple line shows monitoring well 1.

The calibration achieved a RMSE of 0.12 m for hydraulic head and a correlation coefficient (R) of 1.0, indicating acceptable results. The decline in hydraulic heads can be attributed to a drier winter with predominantly solid precipitation (snow) (Figure 8b). The observed data dispersion partly results from local seasonal fluctuations in hydraulic heads.

The model's ability to replicate the hydrogeological behavior of the Quémont 2 TSF was demonstrated through a transient-state simulation. Daily hydraulic head variations were simulated for the period from 5 November 2020 to 3 June 2022. The transient analysis utilized boundary conditions, initial conditions, and material properties derived from the steady-state calibration. Figure 8b presents the results for this period. Additionally, the simulation incorporated the degree-day snowmelt approach to account for the drier winter conditions and the spring snowmelt period, characterized by a significant increase in water input. The degree-day method is a temperature-index approach that relates the total daily melt to the difference between the mean daily temperature and a base temperature (commonly 0 °C), using the following equation:

$$M = CM (T_a - T_b) \quad (4)$$

where  $M$  is the snowmelt (mm/day),  $T_a$  is the mean daily air temperature ( $^{\circ}\text{C}$ ),  $T_b$  is the base temperature ( $^{\circ}\text{C}$ ), and  $CM$  is the degree-day coefficient (mm/degree-day  $^{\circ}\text{C}$ ), which varies seasonally and spatially. Typical values range from 1.6 to 6.0 mm/degree-day  $^{\circ}\text{C}$ . For this study, a value of 2.74 mm/degree-day  $^{\circ}\text{C}$  was used, based on [69].

#### 4.3. Climate Change

Following these calibrations, the model was used to simulate the water resource dynamics of the TSF through the year 2100, considering CC impacts under three different scenarios (RCP 2.6, RCP 4.5, and RCP 8.5).

In these simulations, the primary projected effect of CC on the Quémont 2 TSF is an increase in groundwater levels, mainly driven by higher precipitation rates. The results indicate that the hydraulic heads in both the lower (mine tailing) and upper (rock) hydrogeological units (Figure 9) are clearly hydraulically interconnected.

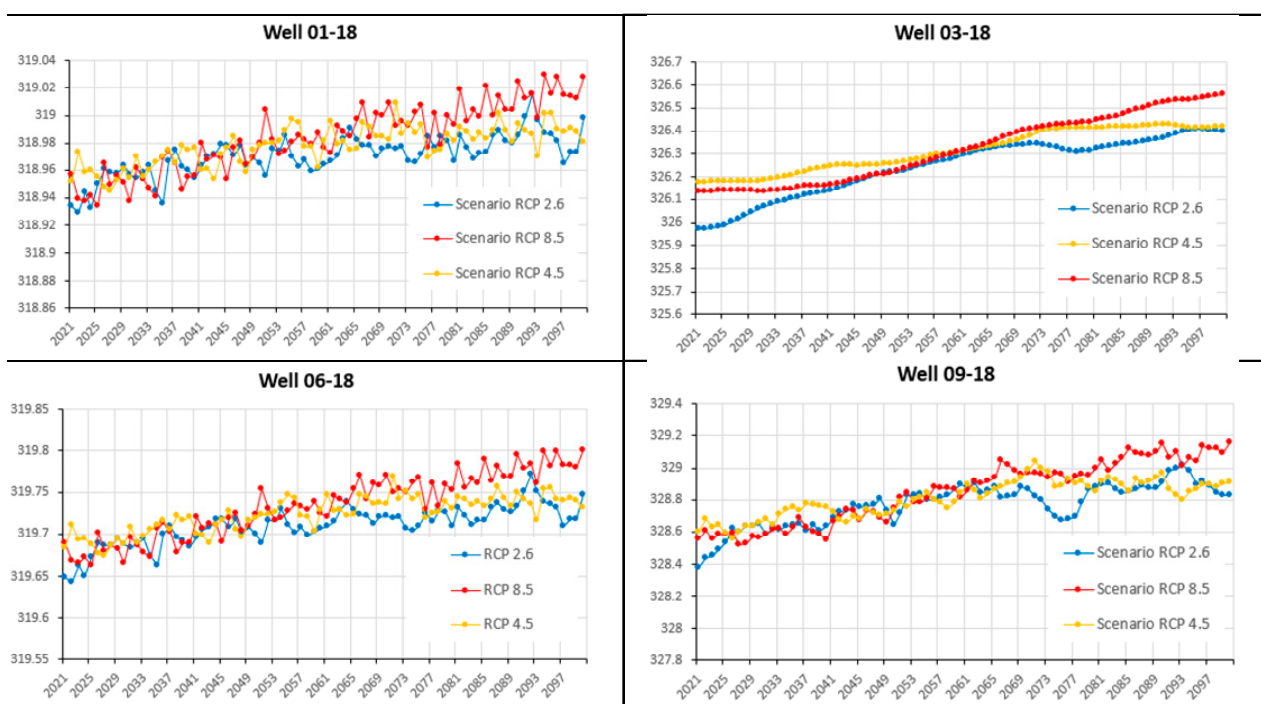


**Figure 9.** Time series of predicted hydraulic heads (in meters) at the Quémont 2 TSF for piezometers 01, 06, and 09 in the mine tailing unit, and piezometer 03 in the Roc Unit.

#### 4.4. Contaminant Transport Using MT3D

A contaminant transport model calculates the concentration distribution of dissolved pollutants in each cell within the model domain based on input parameters and boundary conditions. The transport modeling results are depicted as multiple sets of concentration contours (ranging from 200 mg/L to 2600 mg/L), each representing the simulated pollutant plume at a specific simulation time (Figure 10a).

Sulfate was selected for the initial contaminant transport simulations, as it is considered a conservative tracer unaffected by sorption. Simulating the transport of a tracer pollutant first allows for a better understanding of the contamination source term and dispersion effects without the influence of sorption. The model effectively described the observed sulfate plume evolution in the rock unit (in 2020), achieving an average correlation coefficient of 1, a MAE of 0.34 mg/L, and a RMSE of 0.432 mg/L (Figure 10b).

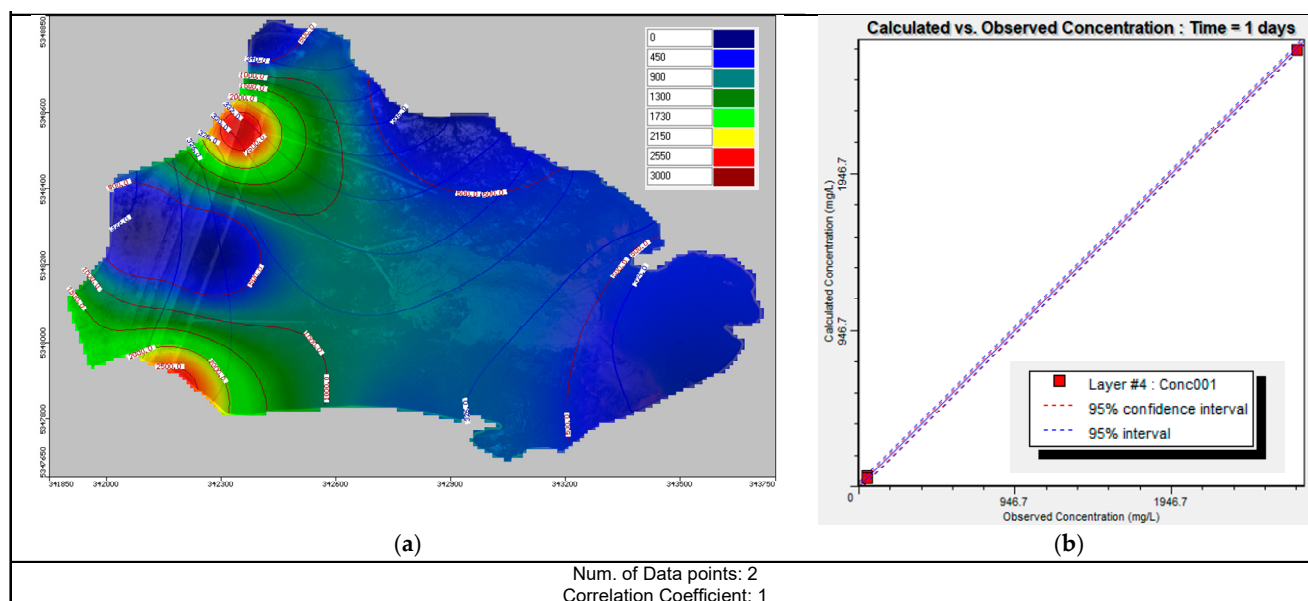


**Figure 10.** (a) Sulfate plume concentration in the Roc Unit of the Quémont 2 TSF (in 2020); (b) calibrated concentration of sulfate plumes comparing estimated and observed values in a scatter diagram.

The abrupt transition to zero concentration in the eastern part of the rock unit appears unrealistic and is likely an artifact resulting from model boundary conditions. It is important to note that this area corresponds to surface water bodies rather than groundwater. Additionally, no concentration measurements were conducted in these surface water bodies in 2020, which may further contribute to the apparent discrepancy. Future simulations should consider these aspects to minimize abrupt transitions and improve the realism of the modeled plume distribution.

Groundwater contamination is primarily attributed to leachate infiltration into the rock unit where the glacio-lacustrine deposits, predominantly composed of clayey silt and clay units, are absent.

From 2020 to 2100, the contaminant plume primarily follows the direction of groundwater flow, with minimal dispersion when moving against the flow. As a result, the solute plume continues to migrate towards the eastern and western boundaries of the model domain (Figure 11a,b). Due to their alignment with the groundwater flow, wells 1 and 3 become progressively contaminated over time (Figure 12). While concentrations in wells 1 and 3 continued to increase throughout the simulation period, the high concentrations in well 2 remained stable from the late 2020s until the end of the simulation in 2100.

#### 4.5. Contaminant Transport Using PHT3D

##### 4.5.1. Copper in Sludge and Slag

In this model, the sludge and slag unit, defined in column 1 for layer 1 (Figure 13), was used to represent the system. Reactive transport simulations were performed for eight components—calcium (Ca), Arsenic (As), Cadmium (Cd), Cobalt (Co), copper (Cu), iron (Fe), lead (Pb), sulfur (S), and zinc (Zn). Cu was identified as the primary contaminating species, while the concentration of the other seven components remained within acceptable levels.

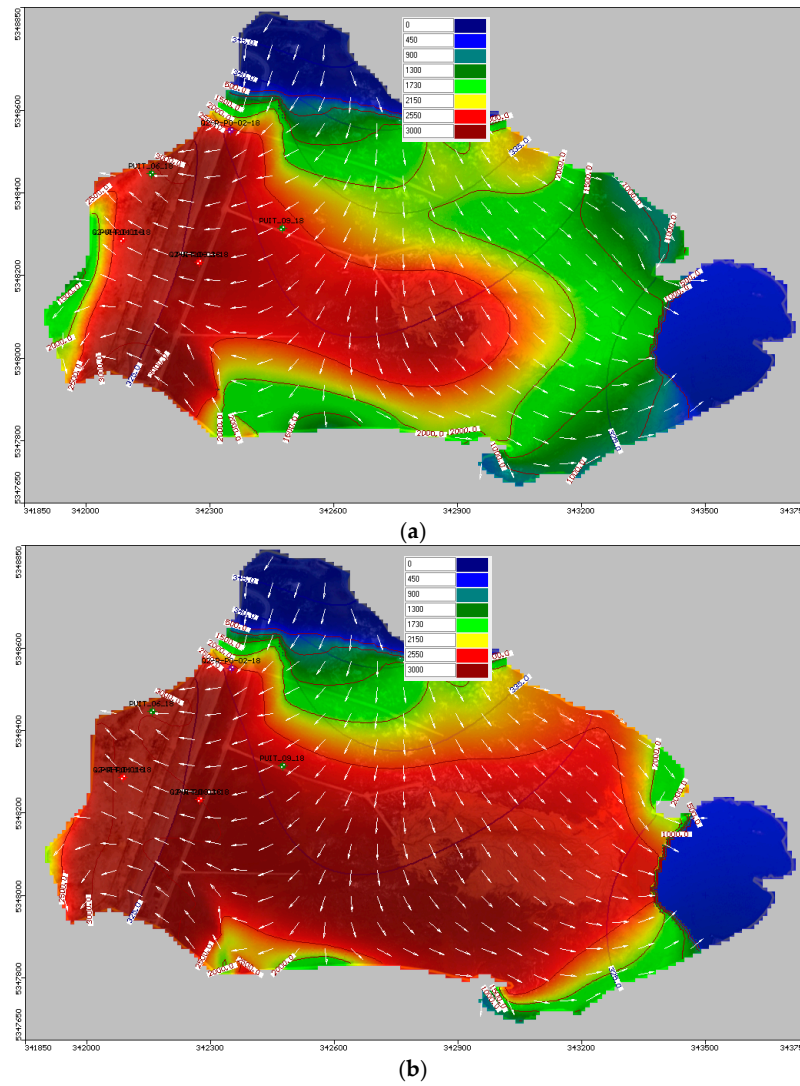


**Figure 11.** Sulfate plume concentration in the Roc Unit of the Quémont 2 TSF (a) in 2050, day = 10,950; and (b) in 2100, day = 29,200. Scenario RCP 2.6.

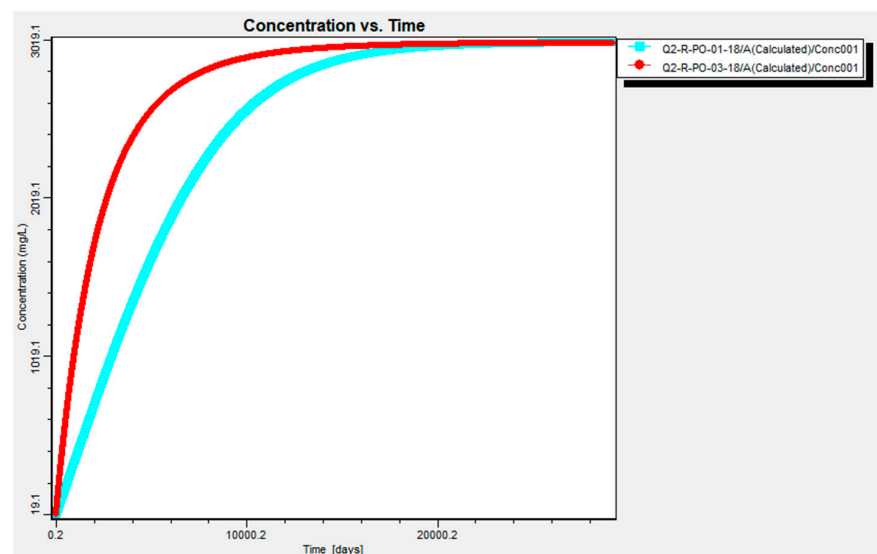


**Figure 12.** Sulfate plume concentration in wells 1 and 3 of the Quémont 2 TSF (from 2020 to 2100), scenario RCP 2.6.

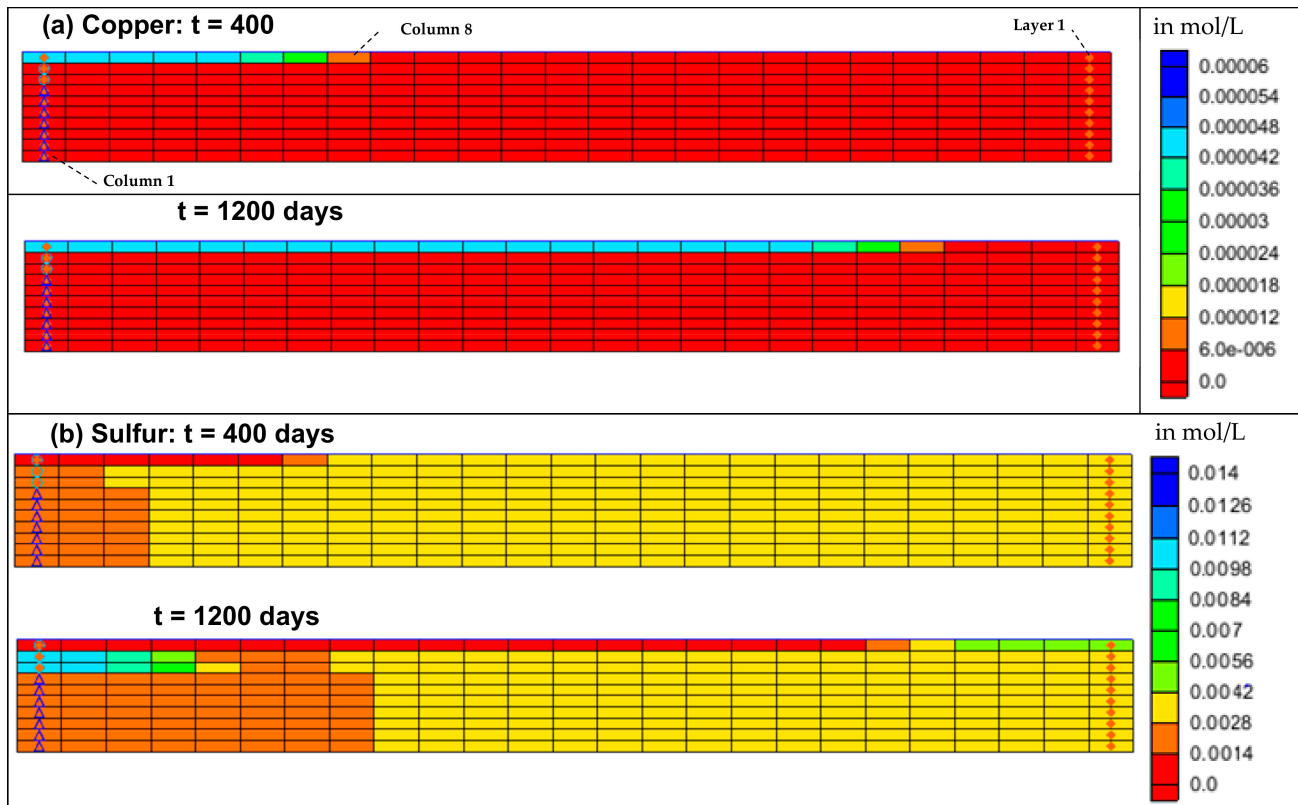


**Figure 13.** Simulated (a) copper and (b) sulfur concentrations after 400 and 1200 days, constant head boundaries (blue symbols) and point source concentrations (orange symbols) were used for in this modeling study as shown in Column 1.

In column 8, the simulated Cu concentrations began to rise during the first 400 days, as shown in Figure 13a. After 400 days, the Cu concentration reached approximately 0.012 mmol/L (0.76 mg/L) and continued to increase, reaching about 0.048 mmol/L (3.05 mg/L) by 1200 days (Figure 13a). After this period, Cu concentrations remained stable until the end of the simulation (7000 days).

#### 4.5.2. Sulfur in Mine Tailing

Additionally, this study focuses on identifying groundwater flow and the transport of two key chemical species—iron (Fe) and sulfur (S)—across the mine tailing site over a 20-year period. AMD is one of the most significant environmental challenges faced by the global mining industry [70]. Pyrite oxidation is a major contributor to AMD formation, releasing iron into the drainage system and contaminating groundwater. These two species were therefore selected for their relevance to this issue [71]. Managing AMD formation remains challenging, particularly in predicting the movement of these chemical species and the generation of pyrite.

Based on the kinetic test conducted by [43], sulfur and iron concentrations were measured using ICP-AES and ICP-MS. The water flush exhibited an iron concentration near or below the detection limit (0.007 mg/L), while sulfur concentration reached 1018 mg/L. As a result, sulfur was identified as the primary contaminant and was defined in column 1 for layers 2 and 3 of the model, representing the mine tailing unit. A sulfur concentration of 0.0313 mol/L was assigned in the model as part of the mineral phases.

In Figure 13b, PHT3D displays concentration values using a color gradient ranging from red to blue, with blue representing the highest concentration. The color profile changes as contamination migrates from the source, illustrating an increase in sulfur concentration within

the mine tailings over 1200 days due to leaching and plume migration. Sulfur concentration values ranged from 0.0014 mol/L to 0.0112 mol/L (equivalent to 134 mg/L to 1056 mg/L).

#### 4.6. Climate Change, Reclamation Technique Using Visual Modflow

After completing calibration, the model was used to simulate the system through the year 2100, incorporating a cover layer on the Quémont 2 TSF. Simulations were conducted under various CC scenarios (RCP 2.6, 4.5, and 8.5). In this final phase, twelve simulations were performed to test different reclamation techniques with varying material properties (Table 6).

**Table 6.** Simulation conducted under CC scenarios and different reclamation techniques.

Reclamation Technique and RCPs	RCP 2.6	RCP 4.5	RCP 8.5
Cell #1: Single layer covering clay (e = 80 cm)	Simulation 1	Simulation 2	Simulation 3
Cell #2: Single layer covering Clay–Sand (e = 60 cm)	Simulation 4	Simulation 5	Simulation 6
Cell #3: Single layer covering Clay–Silt (e = 60 cm)	Simulation 7	Simulation 8	Simulation 9
Cell #4: Multilayer covering Clay–Sand–Clay (e = 40 cm each)	Simulation 10	Simulation 11	Simulation 12

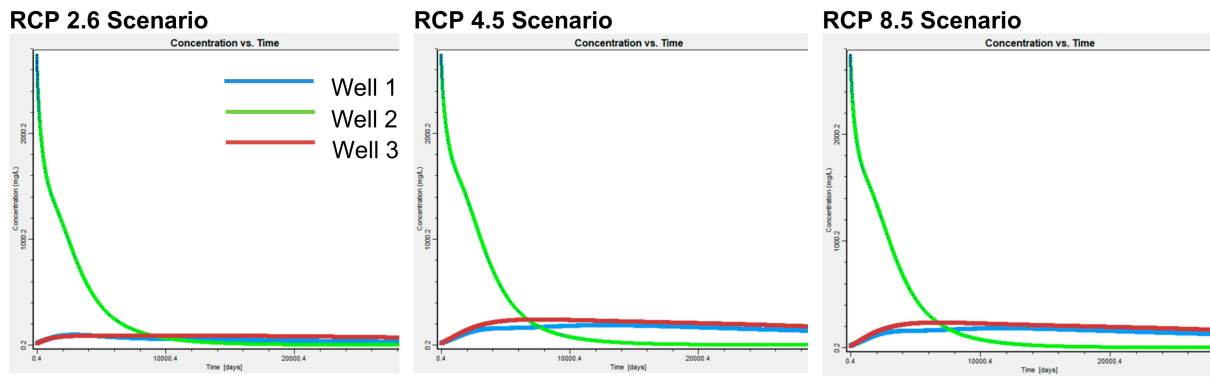
Cell #1, which models a single 80 cm thick clay layer, and Cell #4, representing a multilayer cover composed of clay–sand–clay sequence with a total thickness of 120 cm, shows fewer impacts on renewable resources and water quality in the Quémont 2 TSF compared to Cell #2 and Cell #3. Under the RCP 2.6 scenario, a decrease in contaminant concentration in Well 2 is observed from 2020 to 2047 (Figure 14a,d), with concentrations in wells 1 and 3 remaining near zero. However, under the RCP 4.5 and 8.5 scenarios, concentrations of approximately 240 mg/L are projected to reach wells 1 and 3 by 2030.

The impacts on renewable resources and water quality are more significant in Cell #2 than in Cell #1. Cell #2 models a single layer of clay and sand with a thickness of 60 cm. Under the RCP 2.6 scenario, well 2 shows a decline in contaminant concentration from 2020 to 2058, while concentrations in wells 1 and 3 remain near zero. However, under RCPs 4.5 and 8.5 scenarios, the concentration in well 2 declines over a longer period, from 2020 to 2074, eventually reaching wells 1 and 3.

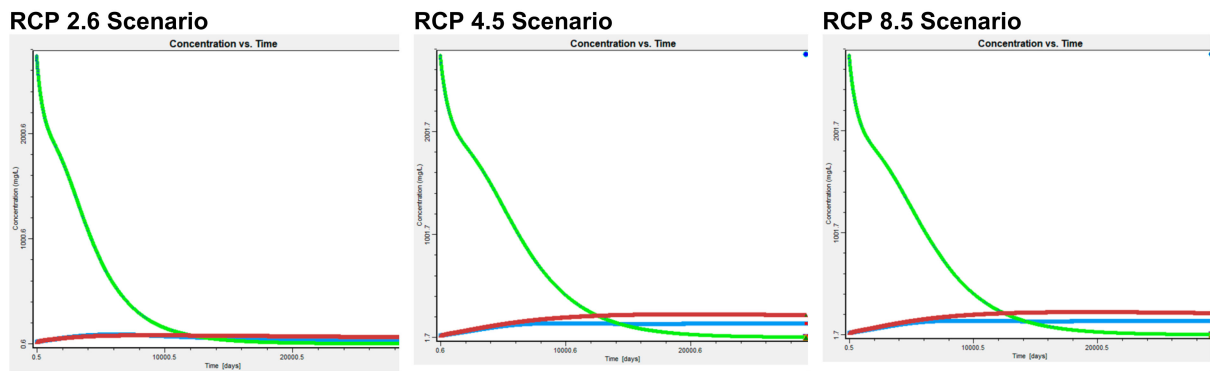
Cell #3, which features a single 60 cm thick layer of clay and silt covering the Quémont 2 TSF, has a greater impact on renewable resources and water quality than Cell #2. In well 2, contaminant concentrations decrease from 2020 to 2052. Under the RCP 8.5 scenario, the most pessimistic case, an increase in hydraulic heads due to CC is observed from 2030 to 2100. Consequently, the solute plume gradually reaches wells 1 and 3 during this period, with expected concentration exceeding 200 mg/L (Figure 14c).

Notably, Cell #1 and Cell #4 demonstrated shorter contamination breakthrough times compared to Cell #2 and Cell #3. In the RCP 4.5 and 8.5 scenarios across all cells (#1, #2, #3, and #4), the observed concentration increases in well 1 and 3 can be attributed to CC impacts, particularly the rise in hydraulic heads caused by increased recharge predictions from 2020 to 2100 in the study area (e.g., the pessimistic RCP 8.5 scenario, Figure 15).

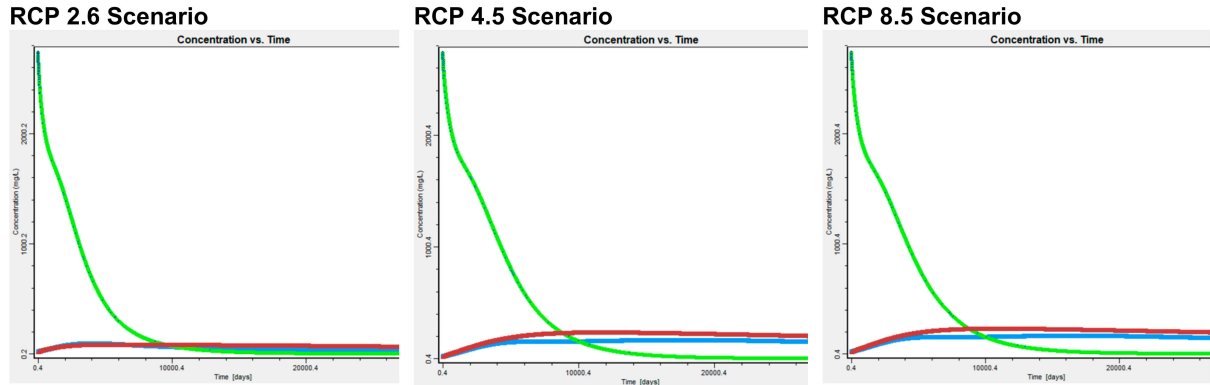
(a) Cell#1: Single layer covering clay (e = 80 cm)



(b) Cell#2: Single layer covering Clay–Sand (e = 60 cm)



(c) Cell#3: Single layer covering Clay–Silt (e = 60 cm)



(d) Cell#4: Multilayer covering Clay–Sand–Clay (e = 40 cm each)

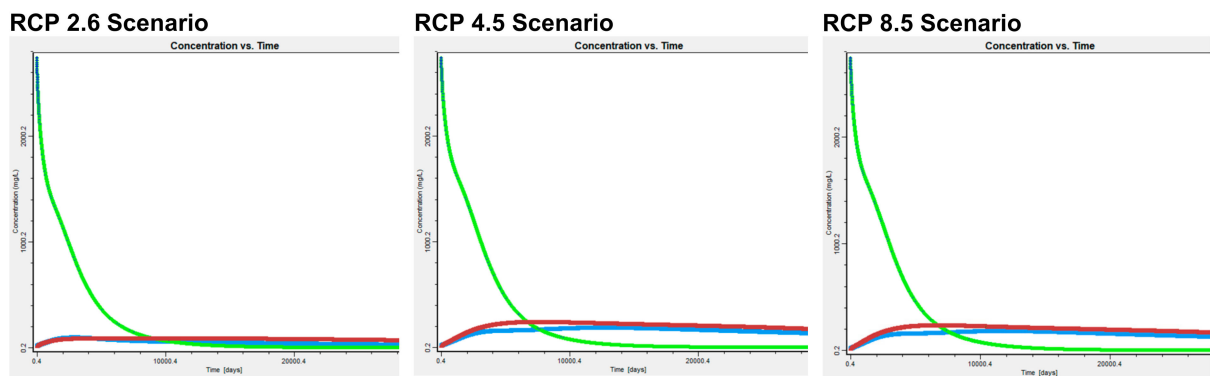


**Figure 14.** Simulated sulfate plume concentration under CC scenarios and different reclamation techniques of (a) Cell #1, (b) Cell #2, (c) Cell #3, and (d) Cell #4.

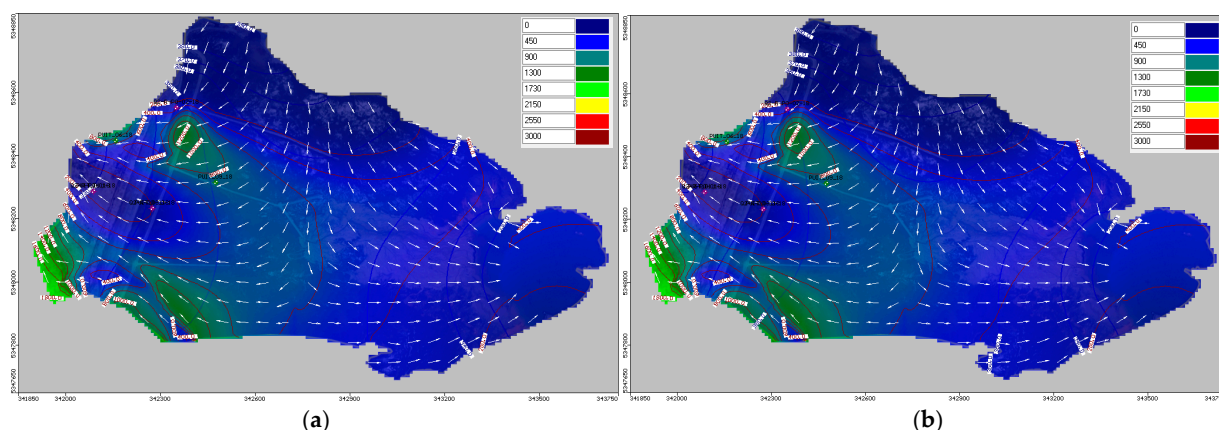


**Figure 15.** Sulfate plume concentration in the Roc Unit of the Quémont 2 TSF after reclamation (a) in 2050, day = 10,950, and (b) in 2100, day = 29,200. Pessimistic scenario RCP 8.5.

Based on these simulations, the most effective reclamation techniques for the mine site are those modeled by Cell #1 and Cell #4. These findings highlight the performance of cover systems placed on the Quémont 2 tailing storage facility.

## 5. Conclusions

The Fonderie Horne is one of Canada's most important copper foundries. Between 1949 and 2018, the Quémont TSF nearly reached its capacity, having received more than 7.6 Mt of sulfide tailings, 14.2 Mt of slag, and 1.1 Mt of sludge. The Quémont TSF, covering approximately 119 ha, presents unique environmental challenges due to the nature of its mine waste and proximity to the metropolitan border of Rouyn-Noranda.

The water table at Quémont 2 exists within a highly heterogeneous complex composed of non-reactive sludge, slag tailings, Quémont 2 tailings, and an underground structural unit (rock and glacio-lacustrine deposits). The site primarily consists of relatively homogeneous rock at the Quémont 2 site, overlain by mine tailings predominantly made of silty materials. In certain areas, an intermediate layer containing glacio-lacustrine deposits (comprising clayey silt and clay units) is intercalated between the rock and mine tailings. This layer can act as a semi-permeable screen, isolating the two underground units (rock and mine tailings).

This study developed a hydrogeological geodatabase organized within a GIS framework. The database contains several information layers related to the aquifer and water resources in the study area, including topography, hydrology, climatology, geology, reservoir geometry, hydrogeology, water quality, and hydrodynamic functioning. These layers were used to produce various decision-making thematic maps such as administrative maps, hydrogeological maps, piezometric maps, and hydrodynamic parameters maps.

Using this database, geostatistical analysis, three-dimensional geometric modeling, and a conceptual model were developed based on newly acquired knowledge. Subsequently, a mathematical three-dimensional groundwater flow and transport model, calibrated under steady and transient conditions, was created using Visual MODFLOW software. The general direction of groundwater flow is from north to east with a component oriented towards the west. Groundwater contamination is mainly due to the leachate infiltration into the rock, especially in areas where glacio-lacustrine deposits (predominantly composed of clayey silt and clay units) are absent.

The establishment of a hydrogeological database and a groundwater model has significantly improved our understanding of the Quémont 2 TSF's hydrogeological properties and hydrodynamic performance, particularly under CC conditions. After calibrating the model in both steady and transient states, linking these results to various CC scenarios was critical for identifying the impacts of CC (precipitation and temperature changes from 2006 to 2100). These results are instrumental in assessing the long-term performance of the TSF and

identifying the most suitable reclamation techniques that site managers should consider for the recovery of the Quémont 2 TSF. The numerical modeling tool has supported the preliminary selection of the best method for mine site reclamation.

The PHT3D model revealed that copper and sulfur in the groundwater remain at excessively high levels. This study enhances our understanding of the reactivity of sulfur generated by mine tailings and the elevated concentrations of copper (Cu) associated with sludge/slag material. These materials contribute to water contamination, posing a significant risk to the quality of the surrounding environment.

The effect of CC on the Quémont 2 TSF is projected to result in increased groundwater levels, primarily due to higher precipitation, especially rain relative to snow. Consequently, a solute plume with concentrations greater than 200 mg/L is expected to gradually reach two observation wells (wells 1 and 3) between 2030 and 2100.

Furthermore, the coupled model indicate that two specific reclamation techniques are most effective the Quémont 2 TSF; a single-layer clay cover (Cell#1) and a multilayer layer cover consisting of a clay–sand–clay sequence (Cell#4). These approaches have demonstrated reduced impacts on renewable resources and improved water quality at the Quémont 2 TSF, making them the most appropriate options for site reclamation.

**Author Contributions:** Conceptualization, M.J.E.H.; Methodology, M.J.E.H. and A.M.; Validation, A.M.; Formal analysis, M.J.E.H.; Writing—original draft, M.J.E.H.; Writing—review & editing, A.M., T.B. and M.-E.V.; Visualization, M.J.E.H.; Supervision, A.M.; Project administration, A.M.; Funding acquisition, A.M. All authors have read and agreed to the published version of the manuscript.

**Funding:** This research was funded by the Fonds de Recherche du Québec sur la Nature et les Technologies (FRQNT), Mitacs, UQAT and the industrial partner Fonderie Horne.

**Data Availability Statement:** Data is contained within the article.

**Acknowledgments:** We extend our gratitude to Glencore Fonderie Horne, Mitacs, FRQNT, UQAT, UQAT Foundation, and the REGENERE institutional chair.

**Conflicts of Interest:** Author Marie-Elise Viger was employed by Fonderie Horne—Glencore. The remaining authors declare that the research was conducted in the absence of any commercial or financial relationships that could be construed as a potential conflict of interest.

## Abbreviations

AMD	Acid Mine Drainage
EWT	Elevated Water Table
CCBE	Cover with Capillary Barrier Effect
TSF	Tailings Storage Facilities
RCP	Representative Concentration Pathway
Mt	Million tons
ha	Hectares
GPR	Ground-Penetrating Radar
EMW	Electromagnetic Waves
ERT	Electrical Resistivity Tomography
DEM	Digital Elevation Model
GIS	Geographic information System
CMIP5	Coupled Model Intercomparison Project 5
CC	Climate Change
Bi-CGSTAB	Bi-Conjugate Gradient Stabilized
RMSE	Root Mean Squared Error
MA	Mean Absolute Error

## References

1. Aubertin, M.; Bussière, B.; Pabst, T.; James, M.; Mbonimpa, M. Review of the reclamation techniques for acid-generating mine wastes upon closure of disposal sites. In Proceedings of the 2nd Geo-Chicago Conference, Chicago, IL, USA, 14–18 August 2016; pp. 343–358.
2. Aubertin, M.; Bussière, B.; Bernier, L. *Environnement et Gestion des Rejets Miniers [Environment and Mine Wastes Management]*; Manual on CD-ROM; Presses Internationales Polytechnique: Montreal, QC, Canada, 2002.
3. Aubertin, M.; Chapuis, R.P.; Aachib, M.; Bussière, B.; Ricard, J.-F.; Tremblay, L. Évaluation en Laboratoire de Barrières Sèches Construites à Partir de Résidus Miniers [Laboratory Evaluation of Dry Covers Constructed from Mine Tailings]. Report NEDEM/MEND. 1995. Available online: <http://www.mend-nedem.org> (accessed on 5 December 2023).
4. Bussière, B.; Aubertin, M.; Zagury, G.J.; Potvin, R.; Benzaazoua, M. Principaux défis et pistes de solution pour la restauration des aires d'entreposage de rejets miniers abandonnées [Key challenges and possible solutions for reclamation of abandoned mine waste storage areas]. In Proceedings of the Symposium 2005 Sur L'environnement et les Mines, Rouyn-Noranda, QC, Canada, 15–18 May 2005.
5. Maqsoud, A.; Bussière, B.; Mbonimpa, M. Low Saturated Hydraulic Conductivity Covers. In *Hard Rock Mine Reclamation: From Prediction to Management of Acid Mine Drainage*; Bussière, B., Guittonny, M., Eds.; CRC Press: New York, NY, USA, 2021.
6. MEND (Mine Environment Neutral Drainage). *MEND Manual, Report 5.4.2, Volume 4—Prevention and Control*; Secretariat CANMET: Ottawa, ON, Canada, 2001.
7. Ritcey, G.M. Tailings Management, Problems and Solutions in the Mining Industry. In *Process Metallurgy 6*; Elsevier: Amsterdam, The Netherlands, 1989.
8. SRK (Steffen Robertson and Kirsten (B.C.) Inc.). *Draft Acid Rock Drainage Technical Guide. Volume I: Report Prepared for British Columbia, Acid Mine Drainage Task Force*; Bi-Tech Publishers Ltd, SRK: Vancouver, BC, Canada, 1989.
9. Amyot, D.; Vézina, S. Flooding as a Reclamation Solution to an Acidic Tailings Pond—the Solbec case. In Proceedings of the 4th International Conference on Acid Rock Drainage, Vancouver, BC, Canada, 31 May–6 June 1997; pp. 681–696.
10. Fraser, W.W.; Robertson, J.D. Subaqueous Disposal of Reactive Mine Waste: An Overview and Update of Case Studies—MEND/Canada. In Proceedings of the International Land Reclamation and Mine Drainage Conference and 3rd International Conference on the Abatement of Acidic Drainage, Pittsburgh, PA, USA, 24–30 April 1994; pp. 250–259.
11. Simms, P.H.; Yanful, E.K.; St-Arnaud, L.; Aubé, B. A laboratory evaluation of metal release and transport in flooded preoxidized mine tailings. *Appl. Geochem.* **2001**, *15*, 1245–1263. [[CrossRef](#)]
12. Aubertin, M.; Pépin, N.; Mbonimpa, M.; James, M.; Prétot, F.; Maknoon, M.; Bussière, B. Vers une mise à jour des critères de stabilité géotechnique pour la conception des ouvrages de retenue de résidus miniers [Towards an update of the geotechnical stability criteria for the design of tailings impoundments]. In Proceedings of the Symposium on Mines and the Environment, Rouyn-Noranda, QC, Canada, 6–9 November 2011. 38p.
13. Aubertin, M.; Dionne, J.; Marcoux, L. Design guidelines and stability criteria of engineering works for water covers. In Proceedings of the 4th ICARD, Vancouver, BC, Canada, 31 May–6 June 1997; pp. 1849–1866.
14. Aubertin, M.; Bussière, B.; Monzon, M.; Joanes, A.M.; Gagnon, D.; Barbera, J.M.; Aachib, M.; Bédard, C.; Chapuis, R.P.; Bernier, L. *Étude sur Les Barrières Sèches Construites À Partir de Résidus Miniers Phase II—Essais En Place [A study of Dry Covers Constructed from Mine Tailings, Phase II: In-Situ Test]*. *Mine Environment Neutral Drainage Report (NEDEM/MEND) 2.22.2c*; CANMET: Ottawa, ON, Canada, 1999; 395p.
15. Dagenais, A.M.; Aubertin, M.; Bussière, B. Parametric study on the water content profiles and oxidation rates in nearly saturated tailings above the water table. In Proceedings of the 7th ICARD, St. Louis, MI, USA, 26–30 March 2006; Barnhisel, R.I., Ed.; The American Society of Mining and Reclamation: St. Louis, MO, USA, 2006; pp. 405–420.
16. Dagenais, A.-M. Techniques de Contrôle du Drainage Minier Acide Basées sur Les Effets Capillaires [Techniques to Control Acid Mine Drainage Based on Capillary Barrier Effects]. Ph.D. Thesis, Polytechnique Montréal, Montreal, QC, Canada, 2005.
17. Demers, I.; Bussière, B.; Benzaazoua, M.; Mbonimpa, M.; Blier, A. Column test investigation on the performance of monolayer covers made of desulphurized tailings to prevent acid mine drainage. *Min. Eng.* **2008**, *21*, 317–329. [[CrossRef](#)]
18. Orava, D.A.; Tremblay, G.A.; Tibble, A.; Nicholson, R. Prevention of acid rock drainage through the application of in-pit disposal and elevated water table concepts. In Proceedings of the 4th ICARD, Vancouver, BC, Canada, 31 May–6 June 1997; pp. 973–983.
19. Ouangrawa, M.; Aubertin, M.; Molson, J.W.; Bussière, B.; Zagury, G.J. Preventing Acid Mine Drainage with an Elevated Water Table: Long-Term Column Experiments and Parameter Analysis. *Water Air Soil Pollut.* **2010**, *213*, 437–458. [[CrossRef](#)]
20. Ouangrawa, M.; Molson, J.; Aubertin, M.; Bussière, B.; Zagury, G.J. Reactive transport modeling of mine tailings columns with capillarity-induced high water saturation for preventing sulfide oxidation. *Appl. Geochem.* **2009**, *24*, 1312–1323. [[CrossRef](#)]
21. Ouangrawa, M. Étude Expérimentale et Analyse Numérique des Facteurs Qui Influencent Le Comportement Hydrogéochimique de Résidus Miniers Sulfureux Partiellement Saturés [Experimental Study and Numerical Analysis of the Factors that Influence the Hydrogeochemical Behavior of Partially Saturated Sulphidic Mining Residues]. Ph.D. Thesis, Polytechnique Montréal, Montreal, QC, Canada, 2007.
22. Ouangrawa, M.; Molson, J.; Aubertin, M.; Zagury, G.J.; Bussière, B. The effect of water table elevation on acid mine drainage from reactive tailings: A laboratory and numerical modeling study. In Proceedings of the 7th International Conference on Acid Rock

- Drainage (ICARD), St. Louis, MO, USA, 26–30 March 2006; Barnhisel, R.I., Ed.; The American Society of Mining and Reclamation: St. Louis, MO, USA, 2006; pp. 1473–1482.
23. Pabst, T.; Aubertin, M.; Bussière, B.; Molson, J. Column tests to characterize the hydrogeochemical response of pre-oxidised acid-generating tailings with a monolayer cover. *Water Air Soil Pollut.* **2014**, *225*, 1–21. [[CrossRef](#)]
  24. SENES. *Review of Use of an Elevated Water Table as a Method to Control and Reduce Acidic Drainage from Tailings*; MEND Report 2.17.1; CANMET: Ottawa, ON, Canada, 1996.
  25. Collin, M. *Mathematical Modeling of Water and Oxygen Transport in Layered Soil Covers for Deposits of Pyritic Mine Tailings*; Royal Institute of Technology: Stockholm, Sweden, 1987.
  26. Cosset, G.; Aubertin, M. Physical and numerical modeling of a monolayer cover placed on reactive tailings. In Proceedings of the 63rd CGC & 1st Joint CGS/CNC-IPA Permafrost Speciality Conference, Calgary, AB, Canada, 12–16 September 2010.
  27. Demers, I.; Bussière, B.; Rousselle, M.; Aubertin, M.; Pabst, T.; Lacroix, R. Laboratory Evaluation of Reclamation Scenarios for the Spillage Areas of the Abandoned Manitou Mine Site Using Goldex Tailings. In Proceedings of the World Mining Congress, Montréal, QC, Canada, 11–15 August 2013.
  28. Dobchuk, B.; Nichol, C.; Wilson, G.W.; Aubertin, M. Evaluation of a single-layer desulphurized tailings cover. *Can. Geotech. J.* **2013**, *50*, 777–792. [[CrossRef](#)]
  29. Ethier, M.P.; Bussière, B.; Aubertin, M.; Maqsoud, A.; Demers, I.; Broda, S. In situ evaluation of the performance of the reclamation measures implemented on an abandoned reactive tailings disposal site. *Can. Geotech. J.* **2018**, *55*, 1742–1755. [[CrossRef](#)]
  30. Maqsoud, A.; Mbonimpa, M.; Benzazoua, M.; Turcotte, S. Evaluation performance of a monolayer cover with an elevated water table used for the reclamation of the abandoned Aldermac mine site (Québec, Canada). *Min. J.* **2022**, *2*, 65–85. [[CrossRef](#)]
  31. Mbonimpa, M.; Aubertin, M.; Aachib, M.; Bussière, B. Diffusion and consumption of oxygen in unsaturated cover materials. *Can. Geotech. J.* **2003**, *40*, 916–932. [[CrossRef](#)]
  32. Cabral, A.; Racine, I.; Burnotte, F.; Lefebvre, G. Diffusion of oxygen through a pulp and paper residue barrier. *Can. Geotech. J.* **2000**, *37*, 201–217. [[CrossRef](#)]
  33. Tassé, N.; Germain, D. Performance of Forestry Wastes for the Treatment of Acid Mine Drainage through a Reactive Barrier. In Proceedings of the 7th International Symposium on Environmental Issues and Waste Management in Energy and Mineral Production (SWEMP 2002), Calgliari, Italy, 7–10 October 2002; pp. 723–773.
  34. Bussière, B.; Maqsoud, A.; Aubertin, M.; Martschuk, J.; McMullen, J.; Julien, M. Performance of the oxygen limiting cover at the LTA site, Malartic, Québec. *Env. Soc. CIM* **2006**, *99*, 1–11.
  35. Collin, M.; Rasmuson, A. Mathematical Modelling of Water and Oxygen Transport in Layered Soil Covers for Deposits of Pyritic Mine Tailings, Acid Mine Drainage: Designing for Closure. In Proceedings of the GAC-MAC Annual Meeting, Vancouver, BC, Canada, 16–18 May 1990; pp. 311–333.
  36. Maqsoud, A.; Bussière, B.; Turcotte, S.; Roy, M. Performance Evaluation of Covers with Capillary Barrier Effects (CCBE) under Deep Groundwater Conditions Using Experimental Cells. In Proceedings of the Conférence Canadienne de Géotechnique, GeoOttawa, Ottawa, ON, Canada, 1–4 October 2017.
  37. Maqsoud, A.; Bussière, B.; Mbonimpa, M.; Aubertin, M.; Chouteau, M. Suction break to control slope-induced effects in covers used as gas barrier. *Can. Geotech. J.* **2011**, *48*, 53–71. [[CrossRef](#)]
  38. Nicholson, R.V.; Gillham, R.W.; Cherry, J.A.; Reardon, E.J. Reduction of acid generation in mine tailings through the use of moisture-retaining cover layers as oxygen barriers. *Can. Geotech. J.* **1989**, *26*, 1–8. [[CrossRef](#)]
  39. WSP. *Modélisation Hydrogéologique Parc À Résidus Actif—Quémont 2*; Glencore Canada Corporation Fonderie Horne: Rouyn-Noranda, QC, Canada, 2019; 296p.
  40. Broda, S.; Aubertin, M.; Blessent, D.; Maqsoud, A.; Bussière, B. Simulating the variation of the phreatic surface level to assess reclamation techniques for an acidic tailings impoundment: A fieldscale study. In Proceedings of the 67th CGS Conference, Regina, SK, Canada, 28 September–1 October 2017. 7p.
  41. Khalil, B.; Broda, S.; Adamowski, J.; Ozga-Zielinski, B.; Donohoe, A. Short-term forecasting of groundwater levels under conditions of mine-tailings recharge using wavelet ensemble neural network models. *Hydrogeol. J.* **2014**, *23*, 121–141. [[CrossRef](#)]
  42. Pabst, T.; Molson, J.; Aubertin, M.; Bussière, B. Physical and geochemical transport modeling of pre-oxidized acid-generating tailings with a monolayer cover. In Proceedings of the 2011 Mine Clos Conference, Lake Louise, AB, Canada, 18–21 September 2011.
  43. El Hamidi, M.J.; Maqsoud, A.; Belem, T. A Kinetic Test Method to Assess the Long-Term Acid Generation Behavior of Sludge/Slag and Mine Tailings of Mine a (Quebec, Canada). In *Recent Research on Sedimentology, Stratigraphy, Paleontology, Geochemistry, Volcanology, Tectonics, and Petroleum Geology. MedGU 2022. Advances in Science, Technology & Innovation*; Springer: Cham, Switzerland, 2024. [[CrossRef](#)]
  44. El-Mrabet, E. Développement D'Approches Géophysiques, D'Imagerie Thermique et de Modélisation pour L'évaluation Des Processus Hydrologiques au Sein D'Un Parc à Résidus Miniers. Master's Thesis, Research Institute on Mines and the Environment (URSTM), Université du Québec en Abitibi-Témiscamingue (UQAT), Rouyn-Noranda, QC, Canada, 2021; 215p.

45. Kahlaoui, S. Évaluation des Échanges Hydrogéo-chimiques Entre un Parc à Résidus Miniers et les Aquifères Périphériques. Master's Thesis, Research Institute on Mines and the Environment (URSTM), Université du Québec en Abitibi-Témiscamingue (UQAT), Rouyn-Noranda, QC, Canada, 2022; 176p.
46. WSP. *Plan de Restauration—Sites Sctifs*; Glencore Canada Corporation—Fonderie Horne: Rouyn-Noranda, QC, Canada, 2019.
47. Granados, A.A.; Maqsood, A.; Belem, T.; Mbonimpa, M.; Viger, M.E. Évaluation sur le terrain de la performance des recouvrements à base d'argile. In Proceedings of the Canadian Geotechnical Conference, GeoCalgary, Calgary, AB, Canada, 2–5 October 2022.
48. Niamké, E.; Maqsood, A.; Belem, T.; Mbonimpa, M. Laboratory assessment of the clay-based covers ability to limit the acid mine drainage production. In Proceedings of the Canadian Geotechnical Conference GeoSaskatoon, Saskatoon, SK, Canada, 1–4 October 2023.
49. Otorola Vasquez, N.C.; Maqsood, A.; Belem, T. Physical and Numerical Modeling of a Flow Control Layer Made with a Sludge and Slag Mixture for Use in Waste Rock Pile Reclamation. *Mining* **2024**, *4*, 841–862. [CrossRef]
50. Données Québec. Database for the Rouyn Region, Québec, Canada. 2022. Available online: <https://www.donneesquebec.ca> (accessed on 15 November 2021).
51. Envirotecheau. Boreholes Logs and Pumping Test Data of the Quémont 2 Tailing Storage Obtained from WSP Report. 1993.
52. SNC LAVALIN. *Boreholes Logs of the Quémont 2 Tailing Storage Obtained from WSP Report*; SNC LAVALIN: Montreal, QC, Canada, 2007.
53. Environment Canada. Climatic Database for the Rouyn Station, Québec, Canada. 2022. Available online: [www.climate.weather.gc.ca](http://www.climate.weather.gc.ca) (accessed on 15 November 2021).
54. Canadian Climate Data and Scenarios. Climate change database for the Rouyn region, Québec, Canada. 2022. Available online: <https://climate-scenarios.canada.ca/?page=statistical-downscaling> (accessed on 15 November 2021).
55. Geocon. *Geotechnical Investigation (Text and Boring Logs)*; Geocon: Lavalin, QC, Canada, 1988; p. 102.
56. URSTM. *Essais Statiques et Cinétiques sur Matériaux de la Fonderie Horne pour Augmentation de Déposition de Résidus*; Unité de Recherche et de Service en Technologie Minérale: Rouyn-Noranda, QC, Canada, 2009; p. 42.
57. Bouwer, H.; Rice, R.C. A slug test method for determining hydraulic conductivity of unconfined aquifers with completely or partially penetrating wells. *Water Resour. Res.* **1976**, *12*, 423–428. [CrossRef]
58. Richelieu. Pumping Test Data of the Quémont 2 Tailing Storage Obtained from WSP Report. 2011.
59. Amec. Pumping Test Data of the Quémont 2 Tailing Storage Obtained from WSP Report. 2014.
60. Environnement Quebec. Directive 019 sur L'Industrie Manière, Québec, Canada. 2012, p. 105. Available online: [https://www.environnement.gouv.qc.ca/milieu\\_ind/directive019/](https://www.environnement.gouv.qc.ca/milieu_ind/directive019/) (accessed on 15 November 2021).
61. Waterloo Hydrogeologic Inc. *Visual MODFLOW User's Manual*; Waterloo Hydrogeologic Inc: Waterloo, ON, Canada, 2022.
62. Harbaugh, A.W.; Banta, E.R.; Hill, M.C.; McDonald, M.G. *MODFLOW-2000, the U.S. Geological Survey Modular Ground-Water Model—User Guide to Modularization Concepts and the Ground-Water Flow Process*; U.S. Geological Survey: Reston, VA, USA, 2000.
63. McDonald, M.G.; Harbaugh, A.W. *A Modular Three Dimensional Finite-Difference Groundwater Flow Model*; Techniques of Water-Resources Investigations Report 06-A1; U.S. Geological Survey: Reston, VA, USA, 1988; 588p.
64. Zheng, C.; Wang, P.P. *MT3DMS: A Modular Three-Dimensional Multispecies Model for Simulation of Advection, Dispersion and Chemical Reactions of Contaminants in Groundwater Systems*; U.S. Army Engineer Research and Development Center: Vicksburg, MS, USA, 1999.
65. Prommer, H.; Barry, D.A. *PHT3D—A Reactive Multi-Component Transport Model for Saturated Porous Media. Version 1.0 User's Manual*; Contaminated Land Assessment and Remediation Research Centre, The University of Edinburgh: Edinburgh, UK, 2001.
66. Parkhurst, D.L.; Appelo, C.A.J. *User's Guide to PHREEQC—A Computer Program for Speciation, Reaction-Path, 1D-Transport, and Inverse Geochemical Calculations*; U.S. Geological Survey Water-Resources Investigations: Reston, VA, USA, 1999.
67. Engesgaard, P.; Kipp, K.L. A geochemical transport model for redox-controlled movement of mineral fronts in groundwater flow systems: A case of nitrate removal by oxidation of pyrite. *Water Resour. Res.* **1992**, *28*, 2829–2843. [CrossRef]
68. Yeh, G.T.; Tripathi, V.S. A critical evaluation of recent developments in hydrogeochemical transport models of reactive multi-chemical components. *Water Resour. Res.* **1989**, *25*, 93–108. [CrossRef]
69. United States Department of Agriculture. Chapter 11: Snowmelt, National Engineering Handbook. Part 630 Hydrology. 2012. Available online: [https://www.irrigationtoolbox.com/NEH/Part630\\_Hydrology/H\\_210\\_630\\_11.pdf#:~:text=This%20chapter%20describes%20the%20basic%20physical%20processes%20that,methods%20may%20also%20be%20used%20for%20short-term%20forecasts](https://www.irrigationtoolbox.com/NEH/Part630_Hydrology/H_210_630_11.pdf#:~:text=This%20chapter%20describes%20the%20basic%20physical%20processes%20that,methods%20may%20also%20be%20used%20for%20short-term%20forecasts) (accessed on 15 December 2022).
70. Akabzaa, T.M.; Armah, T.E.K.; Baneong-Yakubo, B.K. Prediction of acid mine drainage generation potential in selected mines in the Ashanti Metallogenic Belt using static geochemical methods. *Environ. Geol.* **2006**, *52*, 957–964. [CrossRef]
71. Equeenuddin, S.M.; Tripathy, S.; Sahoo, P.K.; Panigrahi, M.K. Geochemistry of ochreous precipitates from coal mine drainage in India. *Environ. Earth Sci.* **2009**, *61*, 723–731. [CrossRef]

**Disclaimer/Publisher's Note:** The statements, opinions and data contained in all publications are solely those of the individual author(s) and contributor(s) and not of MDPI and/or the editor(s). MDPI and/or the editor(s) disclaim responsibility for any injury to people or property resulting from any ideas, methods, instructions or products referred to in the content.